Advances in Applied Energy 19 (2025) 100233

Contents lists available at ScienceDirect

Advances in Applied Energy

journal homepage: www.elsevier.com/locate/adapen

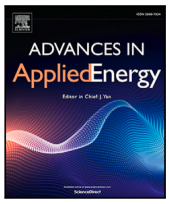

District heating network topology optimization and optimal co-planning using dynamic simulations☆

Jonathan Vieth *, Jan Westphal, Arne Speerforck

Institute of Engineering Thermodynamics, Hamburg University of Technology, Denickestraße 17, Hamburg, 21073, Germany

ARTICLE INFO

Keywords:
District heating
District heating network planning
District heating network simulation
Co-planning
Network routing

ABSTRACT

District heating networks play a critical role in the transition of the heating supply of buildings to renewable sources. The transition from coal-fired or gas-fired generation units to heat pumps requires new planning methods for district heating networks, since the efficiency of a heat pump is affected strongly by the supply temperature of the district heating network. Therefore, a co-planning approach including the operation of the district heating network in the planning process is required. This paper presents a novel co-planning approach consisting of two steps. First, an optimal district heating network topology is generated from real geo-referenced data. To determine the optimal topology, a new algorithm designed specifically for district heating networks is presented. Next, a simulation model is automatically generated from the respective topology. An optimization is used for the co-planning approach to select an optimal generation unit, find the optimal supply temperature, and dimension the pipes of the district heating network. In contrast to conventional district heating network planning procedures, the optimization includes a full-year dynamic simulation of the district heating network. The result of the planning process is a full y parameterized district heating network with a matching supply temperature. Furthermore, the use of simulation models allows the results to be reused for sensitivity analyses. This is illustrated by examining the selection of generation units under different CO_2 price scenarios.

1. Introduction

To meet the targets of the European Green Deal, the heat supply of buildings must be decarbonized by 2050 [1]. A recent study for Germany showed that the share of buildings supplied by DHNs needs to increase to meet the targets [2]. The study considered four scenarios. In three of the four scenarios, the share of houses connected to DHNs in 2045 is at least double the share in 2020.

During the operation of the DHN, the generation units are responsible for the CO_2 emissions of the DHN and need to change accordingly to meet the set targets. One technology that has been the subject of much discussion is heat pumps (HPs) [3]. The efficiency of HPs strongly depends on the supply temperature, i. e. on the operation of the DHN. Therefore, the design of a DHN supplied by at least one HP should include the operation of the DHN in the design process. In [4], the integration of the operation into the design of the energy system is referred to as *co-planning*.

The main goal of this work is to develop a method for optimal DHN design given an area of interest with demand data. The method incorporates investment and operational aspects, i. e. co-planning, and should be able to incorporate the design of the generation unit and the house stations into the planning.

1.1. Related literature

Demand data is often provided in the form of GIS data with house locations and annual heating demand. In [5], the annual heating demand for houses is estimated based on energy archetypes and house characteristics, resulting in a heat cadastre. Eslami et al. [6] present a DHN planning method based on GIS data. The GIS data is used to forecast the heat demand for 2030 and to assess the solar energy potential. The data are then processed using the *EnergyPlan* tool to calculate CO_2 emissions and total annualized cost of the system. EnergyPlan is a tool for planning integrated energy systems that has been developed since 1999 [7]. EnergyPlan calculates annualized costs and yearly CO_2 emissions using a linear model [8] with an hourly time resolution [9]. However, in [6] the DHN losses are calculated using a constant factor rather than a physical relationship, and do not include DHN operation. In [10], a GIS-based model is used to check the feasibility of extending

☆ The short version of the paper was presented at ICAE2024, Niigata, Japan, Sep 1–5, 2024. This paper is a substantial extension of the short version of the conference paper.

* Corresponding author.
E-mail addresses: jonathan.vieth@tuhh.de (J. Vieth), j.westphal@tuhh.de (J. Westphal), arne.speerforck@tuhh.de (A. Speerforck).

https://doi.org/10.1016/j.adapen.2025.100233
Received 22 May 2025; Received in revised form 11 July 2025; Accepted 15 July 2025
Available online 24 July 2025

the DHN in Turin. However, due to the massive size of the DHN, by running a hydraulic simulation of the DHN taken from [11], the expansion is only tested and not optimally planned.

To accurately represent DHN losses, a DHN model consisting of a DHN topology with parameterized pipes is required. Based on a heat cadastre and a generation unit location, a DHN topology can be determined. Fuchs and Müller [12] presented a methodology for creating dynamic DHN models from open street map (OSM). The user selects a generator node and buildings to connect to the DHN. Each building is connected to the generator node by finding the shortest path within the street network, which usually does not result in the shortest DHN topology, as discussed in Section 2.4. Mathematically speaking, the shortest possible topology is a *Steiner tree* [13], for which algorithms are presented in [14,15]. Steiner tree algorithms are utilized in [16] in order to find the optimal DHN topology. However, minimizing the investment cost (i. e. the piping length) without considering the operation is not always beneficial. For the sake of shorter overall DHN topologies, the distance from the generator to the critical consumer may be longer. The critical consumer is the one with the longest piping distance from the generator. This can result in higher pressure losses within the DHN.

As stated in [17], the diameters of future DHNs will have to be smaller in order to increase the overall system efficiency. However, smaller diameters result in higher pressure losses. Therefore, it is necessary to integrate pressure losses into the search for an optimal DHN topology. This task can be solved using mixed-integer programming (MIP) algorithms. A summary of several MIP algorithms is given in [18]. A linear power flow model based on [19] is included in [18] for optimal DHN planning. For a use case with 866 consumers and 2000 streets, the algorithm took more than an hour to compute. A nonlinear model is used in [20]. Although, numerical simplifications such as numerical continuity for discrete diameter values are used, the mixed-integer approach took 46 min for a district with 160 buildings. In [21], the authors were able to improve the computation time of [20] to 10 min by using a pipe diameter penalization approach that achieves near-discrete design. However, this is still slow compared to the approaches presented in [12,16]. The method described in [12] converges within seconds, as will be shown later in Section 4.

According to [22], the pressure control within a DHN depends on the critical consumer. Therefore, keeping the distance from the generator node to the critical consumer as short as possible, while minimizing the overall topology length, would be the perfect approach. The task of finding Steiner trees with additional constraints is usually framed as the search for a *constrained Steiner tree* [23]. However, to the best of the authors' knowledge, there is no algorithm for finding a Steiner tree where the distance from a generator node to all consumer nodes is either constrained or minimized.

Since the goal is to incorporate the design and the operation of the generation unit into the planning, it is not sufficient to consider only the worst-case load situation. In the case of DHN planning, there are two approaches to the co-planning of DHNs [24]. The first approach formulates the co-planning problem as a MIP, where the physics behind the DHN are contained in the constraints of the optimization problem. The MIP approaches are usually validated either with small districts (twelve houses in [25], resulting in more than 80 000 planning variables) or by simplifying the physics of the DHN. For example, in [26] the spatial resolution of the DHN is omitted, and in [27] the network losses are omitted to obtain a linear optimization model. Wirtz et al. [28] present an optimization procedure for the design of a 5th generation DHN. To obtain a linear model, the DHN is modeled using a power balance. In [29], an *energy hub* (EH) model and linear optimization are used for co-planning a DHN. An EH is a simplified modeling concept for integrated energy systems, as introduced in [30]. It describes the transformation, storage, and consumption of energy in one centralized unit, the EH. However, an EH does not model a DHN in detail; e. g., it does not use physical pipe models. Hence, heat losses can only be estimated.

A second approach is used in [31], where the DHNs are simulated for a representative time interval and the results of the simulation are processed by a genetic algorithm. The second approach has several advantages. First, as pointed out in [31], only a simulation can handle the complex restrictions typically present in DHNs without significantly increasing the mathematical complexity. Examples of constraints are the bang–bang control of hot water storage tanks or the pressure control of the critical consumer. Second, as long as the simulations do not require cost data, which is usually the case since investment and fuel costs are needed after the simulation, the simulation results can be stored and reused for other cost scenarios, which is important in energy systems due to the uncertainty of future fuel and investment prices.

A review of DHN planning tools [32] concluded that none of the analyzed tools use thermodynamic models for DHN planning. Kuntuarova et al. [33] analyzed simulation tools, such as *Pandapipes* [34], *TRNSYS* [35], *STANET* [36], and *Dymola* [37], and planning tools, such as *EnergyPlan* [7] and *nPro* [29]. As mentioned above, *EnergyPlan* does not use implicit DHN component models and *nPro* only allows steady-state analysis [33].

In conclusion, there are several approaches for co-planning DHNs. However, there is a lack of fast algorithms for DHN optimization including operational aspects. Furthermore, none of the analyzed planning methods use dynamic full-year DHN simulations without oversimplifying the DHN.

1.2. Contribution

The contribution of this work is twofold. First, it presents a fast and novel algorithm for finding the optimal DHN topology. The algorithm determines the optimal topology not only by minimizing the total piping length but also by minimizing the distance from the generation unit to the critical consumer. The first objective is relevant for minimizing the investment cost, while the second influences the operating cost of the DHN. The algorithm yields an optimal topology within seconds, taking into account the operational behavior. The second contribution is a framework for a detailed co-planning using a surrogate optimization and dynamic simulations of the DHN and the connected houses. This allows not only the consideration of operational variables such as heat and pressure losses, but also the investigation of dynamic effects such as the inertia of decentralized heat storage.

The contribution of this work is in summary:

- a new algorithm that enables a trade-off between investment and operating cost for finding the optimal topology from a set of possible routes specialized for DHNs
- a tool-chain for the optimal co-planning of DHNs, including a full-year dynamic simulation of the DHN and the connected houses
- a case study including
  - a comparison of different domestic hot water supply methods
  - a scenario analysis with varying CO_2 prices

2. Automated simulation model generation

The procedure for finding the optimal DHN configuration is shown in Fig. 1. As presented in Section 1.2, the planning process consists of two steps: First, finding the optimal topology, and second, simulating the DHN within an optimization. This section presents an automated framework for DHN simulation model generation including the new algorithm that allows a trade-off between investment and operational costs to find the optimal DHN topology, which is one of the main contributions.

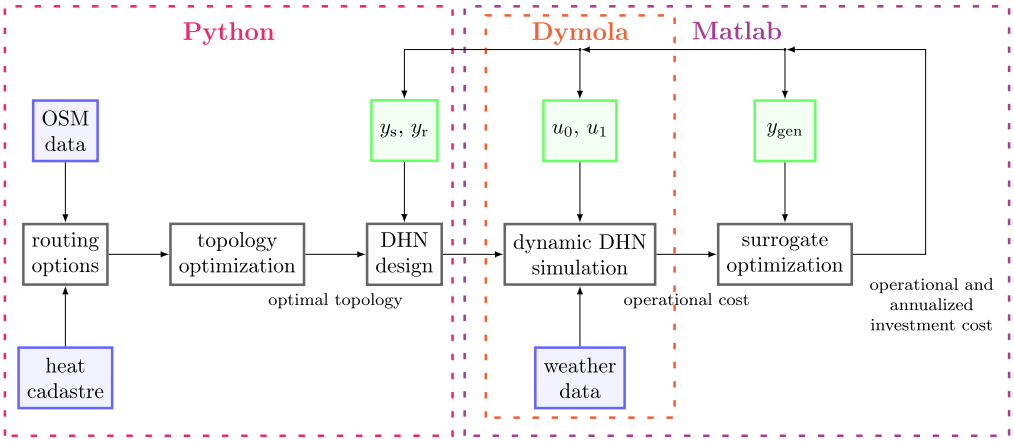

Fig. 1. DHN optimization procedure, including the software tools used. Design variables in green (explained in Section 2.1) and area dependent inputs in blue. (For interpretation of the references to color in this figure legend, the reader is referred to the web version of this article.)

2.1. Design variables

For the parameterization and simulation five design variables

$$z = \begin{bmatrix} u_0 & u_1 & y_s & y_r & y_{gen} \end{bmatrix}^\top \tag{1}$$

are used. The two variables u_0 and u_1 are the operational planning variables. Both variables effect the supply temperature of the DHN, as described in more detail in Section 3.2.2. The expansion planning variables are y_s, y_r, and y_{gen}. The first two are target pressure losses as presented in [38] and are used for sizing the supply pipes and the return pipes, respectively, as discussed in Appendix A.2. Choosing smaller diameters for the supply pipes than for the return pipes may be an optimal choice because the supply temperatures are higher and therefore the trade-off between heat losses and pressure losses may lead to smaller diameters in a supply pipe than in a return pipe. The last variable y_{gen} is the choice of generation unit.

2.2. Input data

The inputs to the network generation are the OSM data [39] and the heat cadastre of the area of interest, shown in blue in Fig. 1. OSM data is used in the form of an undirected graph $\mathcal{G}_{osm}\left(\mathcal{N}_{osm}, \mathcal{E}_{osm}\right)$ with nodes $\mathcal{N}_{osm}$ and edges $\mathcal{E}_{osm}$ accessed by using the *OSMnx* package [40]. In contrast to using data from local authority, global data is available making tools based on OSM reusable in various locations. Hence, OSM data is often used for generating energy network models [41].

The heat cadastre can be thought of as a table with one row for each building $b \in \mathcal{B}$, where $\mathcal{B}$ is the set of buildings. The columns are the building locations, the yearly heating demand Q_b, and the maximum required heating power $\dot{Q}^b_{max}$.

2.3. Routing options

To find the optimal DHN topology, the buildings must be connected to the street network. This is achieved by creating a copy $\mathcal{G}_{rou}\left(\mathcal{N}_{rou}, \mathcal{E}_{rou}\right)$ of $\mathcal{G}_{osm}$. Then, each building $b \in \mathcal{B}$ is iteratively added to $\mathcal{G}_{rou}$ by finding the closest point p on any edge in $\mathcal{E}_{rou}$ and adding an edge to $\mathcal{G}_{rou}$ that connects b with p. The same procedure is conducted for the location of the generation unit. Thus, $\mathcal{N}_{rou}$ can be decomposed into the set of building nodes $\mathcal{N}_b$, the set of generator nodes $\mathcal{N}_{gen}$, and the set of street crossings $\mathcal{N}_{cro}$.

2.4. Topology optimization

The routing options for the DHN are defined by $\mathcal{G}_{rou}$. Next, for each edge $e \in \mathcal{E}_{rou}$, it must be decided whether e is part of the optimal DHN topology described by the graph $\mathcal{G}_{dhn}\left(\mathcal{N}_{dhn}, \mathcal{E}_{dhn}\right)$. From a graph theoretical point of view, the goal is to connect a set of terminal nodes $\mathcal{N}_{term} = \mathcal{N}_b \cup \mathcal{N}_{gen}$ to each other through the optimal edges $\mathcal{E}_{dhn} \subseteq \mathcal{E}_{rou}$. In case the goal is to find G_{dhn} with minimum length, G_{dhn} is a *Steiner minimal tree*. The following sections present three approaches for finding $\mathcal{G}_{dhn}$. The approach presented in Section 2.4.1 comes from [16], and the approach in Section 2.4.2 from [12]. Section 2.4.3 discusses the newly developed *constrained Steiner tree algorithm*, which is specifically designed for DHNs and is one of the contributions of this work integrating operational aspects into DHN planning.

2.4.1. Steiner tree

The *Steiner minimal tree* is the subgraph $\mathcal{G}_{st}\left(\mathcal{N}_{st}, \mathcal{E}_{st}\right)$ of $\mathcal{G}_{rou}$ such that $\ell_\sum(\mathcal{G}_{st}) = \sum_{e\in\mathcal{E}_{st}} \ell(e)$ is smaller than the total distance $\ell_\sum$ of any other tree of $\mathcal{G}_{rou}$ connecting the nodes in $\mathcal{N}_{term}$ with each other [13]. Here, $\ell(e)$ is the length of edge e. There are two algorithms for finding the Steiner minimal tree in *networkX* [42], the algorithms by Kou [14] and by Mehlhorn [15]. The main advantages of using the Kou or Mehlhorn algorithms to find $\mathcal{G}_{dhn}$ are, first, that the problem is well studied and therefore already implemented, for example, in the Python library *networkX*. Second, the total distance $\ell_\sum$ is close to or equal to the shortest possible distance. However, this is not always beneficial when controlling the DHN. The pressure within a DHN is controlled in order to achieve a minimum pressure difference at each house station of the DHN [22]. Assuming that the DHN has a single pump at the generator park to control the mass flow, the required pumping power P_{pu} of the pump depends on the pressure drop between the generator park and the critical consumer with the lowest pressure difference at the house station. Apart from the diameter of the pipes and the mass flow in the pipes, the main influence on the pressure loss and therefore on P_{pu} is the pipe length ℓ_{cc} between the generator park and the critical consumer. Therefore, from a pressure control perspective, it may be advantageous to accept higher values for $\ell_\sum$ in order to decrease ℓ_{cc}.

In addition, the temperature in the network decreases as the water travels to the consumer. Since a consumer requires a certain water temperature to extract heat from the network, the longer the travel time to the critical consumer, the higher the required supply temperature at the generator. The travel time is influenced by the water mass flow and the distance from the generator to the critical consumer. Since the pressure loss in the network increases with the mass flow, very high mass flows are not advantageous [38]. Therefore, from a temperature control perspective, it may as well be beneficial to accept higher values for $\ell_\sum$ in order to decrease ℓ_{cc}.

The aforementioned goal can be formulated as an optimization problem

$$\min_{\mathcal{G}_{dhn}} \ell_\sum\left(\mathcal{G}_{dhn}\right), \tag{2a}$$

s. t. (2b)

$$\mathcal{N}_{\text{term}} \subseteq \mathcal{N}_{\text{dhn}}, \tag{2c}$$

$\mathcal{G}_{\text{dhn}}$ is connected, (2d)

$$\ell_n \leq \ell_{\max} \quad \forall n \in \mathcal{N}_{\text{b}}, \tag{2e}$$

where the objective (2a) defines the goal to minimize the supply piping length, (2c) the constraint that all consumers and generators are part of the network, (2d) the constraint that exactly one DHN connects the generators to the consumers, and the constraint (2e) that the distance from the generator to any consumer node n is not higher than $\ell_{\max}$. Two algorithms for solving (2) are described in the two following sections.

2.4.2. Shortest path search

A first simple and fast algorithm for solving (2) was presented in [12] and is described by Algorithm 1 in Appendix A.1. The algorithm searches for $\mathcal{G}_{\text{dhn}}$ by finding the shortest path in $\mathcal{G}_{\text{rou}}$ from g to each $n \in \mathcal{N}_{\text{term}} \setminus \{g\}$. In contrast to Kou's algorithm, the shortest path calculations in between two nodes $n_i, n_j \in \mathcal{N}_{\text{term}}$ are omitted, since otherwise constraint (2e) is not guaranteed to be satisfied. Therefore, the algorithm ensures that the shortest path in $\mathcal{G}_{\text{dhn}}$ from the generator to any consumer node is equal to the shortest path in $\mathcal{G}_{\text{rou}}$.

2.4.3. Constrained Steiner algorithm

The shortest path algorithm guarantees to satisfy all constraints (2c)–(2e). However, as discussed later in Section 4.1, the optimal objective value is disappointing compared to Kou's algorithm. The reason for the poor performance of Algorithm 1 is that the algorithm does not search for shortest paths between two nodes $n_i, n_j \in \mathcal{N}_{\text{term}} \setminus \{g\}$ even if a direct connection between n_i and n_j would not violate constraint (2e).

The algorithm described in Appendix A.1 by Algorithm 2 fills this gap. In a first step, the consumer node with the longest distance $\ell_{\text{sp,max}}$ to the generator is identified, assuming that all consumers are connected to the generator by shortest path search. The distance $\ell_{\text{sp,max}}$ is equal to ℓ_{cc} resulting from algorithm 1. Next, a flexibility factor $\beta \geq 1$ is introduced to calculate $\ell_{\max} = \beta \ell_{\text{sp,max}}$. The factor β can be understood as a parameter for a trade-off between the two goals of achieving a low $\ell_{\sum}$ and achieving a low ℓ_{cc}.

At the beginning of the algorithm, $\mathcal{G}_{\text{dhn}}$ consists only of the generator node g. Next, the buildings with their optimal paths are iteratively connected to $\mathcal{G}_{\text{dhn}}$. The building node r that results in the lowest added piping length

$$p(r) = \sum_{e \in \mathcal{E}_r} \ell(e) \tag{3a}$$

and satisfies

$$\sum_{e \in \hat{\mathcal{E}}_r} \ell(e) \leq \ell_{\max} \tag{3b}$$

is added first. Here, $\mathcal{E}_r$ is the shortest path from any node in $\mathcal{N}_{\text{dhn}}$ to r and $\hat{\mathcal{E}}_r$ is the shortest path from g to r if $\mathcal{E}_r$ is added to $\mathcal{G}_{\text{dhn}}$. If no shortest path $\mathcal{E}_r$ satisfies (3), a path has to be found that is minimal in additional pipe length but satisfies constraint (2e). This is done by an iterative shortest path search with respect to the weighted cost

$$w(e) = \epsilon \ell(e) + (1 - \epsilon) c(e), \quad \forall e \in \mathcal{E}_{\text{rou}}, \tag{4}$$

where

$$c(e) = \begin{cases} 0, & \text{if } e \in \mathcal{E}_{\text{dhn}}, \\ \ell(e), & \text{else.} \end{cases} \tag{5}$$

and $\epsilon = \Delta\epsilon$. First, the shortest path $\mathcal{E}_r$ from g to any unprocessed consumer node r is computed with edge weight w. If $\mathcal{E}_r$ does not satisfy (3), ϵ is increased by $\Delta\epsilon$ and the shortest path search is performed again with the newly computed w as edge weight.

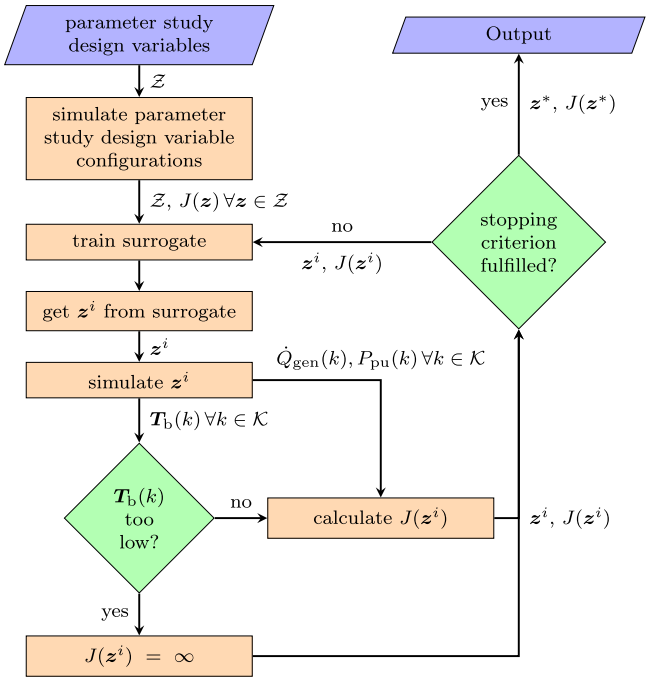

Fig. 2. Procedure of the surrogate optimization algorithm.

3. Optimization

Heendeniya et al. [4] divide the planning process into *expansion planning* and *operation planning* and frame the combination of both aspects *co-planning*. The first step of the *expansion planning* process was performed in Section 2 by finding the optimal DHN topology. The second step of *expansion planning*, which includes *operation planning*, consists of dimensioning the pipe diameters and selecting a generation unit. This is achieved through the optimization procedure shown in Fig. 2. In a parameter study, a dynamic DHN simulation for various $\boldsymbol{z}$ combinations is performed ($\boldsymbol{z}$ is defined in Section 2.1). Each simulation results in the required heating demand $\dot{Q}_{\text{gen}}(k)$ of the DHN at the generator, a vector of the building temperatures $\boldsymbol{T}_{\text{b}}(k)$, and the required pumping power $P_{\text{pu}}(k)$ of the main DHN pump for each time step $k \in \mathcal{K}$, where $\mathcal{K}$ is the set of all time steps spanning a whole year. Based on the simulation results, a cost function $J(\boldsymbol{z})$ consisting of annualized investment and yearly operation cost is calculated. Afterwards, a surrogate function imitating the relationship between $\boldsymbol{z}$ and J is trained. This surrogate function serves as a starting point for the surrogate optimization. In each iteration i of the optimization, the surrogate function suggests a new $\boldsymbol{z}^i$ value, which is then used to simulate the DHN resulting in a matching $J(\boldsymbol{z}^i)$ that is once again used to train the surrogate. The optimization results in an optimal design variable configuration $\boldsymbol{z}^*$ and a matching minimum cost function $J(\boldsymbol{z}^*)$. A detailed explanation of each step of the optimization is provided in the following sections.

3.1. Parameter study

A parameter study is performed to validate the simulation models and gain a better understanding of how design variables affect the efficiencies and costs of the DHN. First, the DHN is simulated using a specified set of design variables $\mathcal{Z} = \{\boldsymbol{z}_1, \boldsymbol{z}_2, \dots\}$. After each simulation j, $J(\boldsymbol{z}_j)$ is calculated for all generator options. The generator types considered in this work are a heat pump (HP), a gas-fueled combined heat and power unit (CHP), and a serial interconnection of a HP and a CHP, as depicted in Fig. B.14. For the parameter study, y_{s} and y_{r} values ranging from $400\,\text{Pa}\,\text{m}^{-1}$ to $2000\,\text{Pa}\,\text{m}^{-1}$ are considered, which

aligns with the results from [38]. Furthermore, u_0 values between 70 °C and 110 °C and u_1 values between 0 and −5 are considered for supply temperature control.

3.2. Dynamic simulation

The simulation is affected by $\boldsymbol{z}$, since y_s and y_r specify the pipe diameters (Appendix A.2). Additionally, operation planning involves altering the two design variables u_0 and u_1, as described in 3.2.2.

3.2.1. Component models

In order to adequately model the dynamic behavior of the buildings, the heating system of the houses, and the DHN itself, a simulation environment that considers the dynamic behavior of the systems has to be invoked. Westphal et al. [43] presented a toolbox for dynamic simulations of DHNs using the modeling language *Modelica*; the toolbox is used in this work. However, the component modeling the generation unit and the component modeling the buildings are adapted to analyze the effect of hot water demand and the effect of varying the DHN supply temperature. Appendix B describes the details of all used models.

3.2.2. Operation planning

In DHNs, *rule-based controllers* are typically used to control the supply temperature $T^{\mathrm{s}}_{\mathrm{gen}}$ at the generation unit [22]. Similar to the control curves of the building radiator systems (Appendix B.3), the control of $T^{\mathrm{s}}_{\mathrm{gen}}$ is based on the outdoor temperature T_{od} [22]. In order to obtain realistic results, a typical DHN control curve [22]

$$T^{\mathrm{s}}_{\mathrm{gen}}(k) = \min\left\{\max\left\{u_0 + u_1 T_{\mathrm{od}}(k), T^{\mathrm{s}}_{\mathrm{min}}\right\}, T^{\mathrm{s}}_{\mathrm{max}}\right\} \tag{6}$$

is used with the two design variables $u_0 \in \mathbb{R}_{>0}$ and $u_1 \in \mathbb{R}_{\leq 0}$. The parameter u_0 can be understood as the supply temperature in the case of $T_{\mathrm{od}} = 0\,°\mathrm{C}$ and u_1 controls the influence of T_{od} on $T^{\mathrm{s}}_{\mathrm{gen}}$. The lower u_1, the greater the variation of $T^{\mathrm{s}}_{\mathrm{gen}}$ with T_{od}. The supply temperature $T^{\mathrm{s}}_{\mathrm{gen}}$ is constrained by the minimum supply temperature $T^{\mathrm{s}}_{\mathrm{min}}$ and the maximum supply temperature $T^{\mathrm{s}}_{\mathrm{max}}$.

The yearly operation cost

$$J_{\mathrm{opt}} = \sum_{k\in\mathcal{K}} \Delta t \left(c_{\mathrm{ele}}(k) P_{\mathrm{ele}}(k) + c_{\mathrm{gas}} P_{\mathrm{gas}}(k)\right) \tag{7}$$

depends on the gas power demand P_{gas} from the CHP and the electric power demand

$$P_{\mathrm{ele}}(k) = P_{\mathrm{pu}}(k) + P_{\mathrm{hp}}(k) - P_{\mathrm{chp}}(k), \tag{8}$$

where P_{chp} and P_{hp} are the electric power generation and demand of the CHP and the HP, respectively. The electric energy price c_{ele} is assumed to be time-dependent (see Appendix C), while the gas price

$$c_{\mathrm{gas}} = 19.4\,€\,\mathrm{MW}^{-1}\,\mathrm{h} + 0.201\,\mathrm{t}\,\mathrm{MW}^{-1}\,\mathrm{h}\, c_{\mathrm{CO_2}} \tag{9}$$

is assumed to be constant, with $c_{\mathrm{CO_2}}$ the CO_2 price and data taken from [44].

The choice of generation unit affects the investment and operating costs of the DHN. If a single CHP or a single HP is used to supply $\dot{Q}_{\mathrm{gen}}$, the equations to calculate P_{hp}, P_{chp}, and P_{gas} are given in Appendix B. Otherwise, a procedure is required to calculate the heating power $\dot{Q}_{\mathrm{hp}}$ of the HP and the heating power $\dot{Q}_{\mathrm{chp}}$ of the CHP with $\dot{Q}_{\mathrm{gen}}(k) = \dot{Q}_{\mathrm{hp}}(k) + \dot{Q}_{\mathrm{chp}}(k)$. The serial configuration with all required variables is shown in Fig. B.14. The optimal $\dot{Q}_{\mathrm{hp}}$ and $\dot{Q}_{\mathrm{chp}}$ are calculated by solving an optimization problem for each time step k. The objective is given by

$$J_{\mathrm{hp,chp}}(h_{\mathrm{hp}}) = J_{\mathrm{chp}}(h_{\mathrm{hp}}) + J_{\mathrm{hp}}(h_{\mathrm{hp}}), \tag{10a}$$

$$J_{\mathrm{hp}}(h_{\mathrm{hp}}) = \Delta t \frac{c_{\mathrm{ele}}(k)}{\mathrm{COP}(h_{\mathrm{hp}})} \dot{Q}_{\mathrm{hp}}(h_{\mathrm{hp}}), \tag{10b}$$

$$J_{\mathrm{chp}}(h_{\mathrm{hp}}) = \Delta t \left(\frac{c_{\mathrm{gas}}}{\eta_{\mathrm{gth}}} - \frac{\eta_{\mathrm{gtp}}}{\eta_{\mathrm{gth}}} c_{\mathrm{ele}}(k)\right) \dot{Q}_{\mathrm{chp}}(h_{\mathrm{hp}}) \tag{10c}$$

with

$$h_{\mathrm{hp}} = h^{\mathrm{r}}_{\mathrm{gen}} + \frac{1}{\dot{m}_{\mathrm{gen}}} \dot{Q}_{\mathrm{hp}}, \tag{10d}$$

$$\dot{Q}_{\mathrm{chp}} = \dot{m}_{\mathrm{gen}} \left(h^{\mathrm{s}}_{\mathrm{gen}} - h_{\mathrm{hp}}\right), \tag{10e}$$

and the COP given by (B.13) with $T_{\mathrm{hp}} = \frac{1}{2}\left(\frac{h_{\mathrm{hp}}}{c_{\mathrm{w}}} + \frac{h^{\mathrm{s}}_{\mathrm{gen}}}{c_{\mathrm{w}}}\right)$ resulting in an optimal h_{hp} for each time step k. The optimization problem (10) is solved using the *interior-point* optimization algorithm from *Matlab*. Therefore, for each time step, $\dot{Q}_{\mathrm{hp}}$ and $\dot{Q}_{\mathrm{chp}}$ result from the simulation and the operation planning.

3.3. Cost calculation

The objective of the co-planning is given by $J = J_{\mathrm{opt}} + J_{\mathrm{inv}}$ with the annualized investment cost $J_{\mathrm{inv}} = \sum_{a\in\{\mathrm{pu,pi,gen,hs}\}} A_a$, where A_{pu}, A_{pi}, A_{gen}, and A_{hs} are the annualized investment costs of the DHN pump, the pipes, the generating unit, and the house stations. The annualization method and assumptions used to calculate the investment costs are described in Appendix C.

3.4. Constraints

The goal of a DHN is to supply buildings with heat. Hence, it is required that the building indoor temperature T_{b} is at each time step k in an acceptable range. Therefore, simulations where $T_{\mathrm{b}} < 20\,°\mathrm{C}$ for more than 20 time steps or $T_{\mathrm{b}} \leq 15\,°\mathrm{C}$ at any time step $k \in \mathcal{K}$ are not considered by the optimization algorithm as feasible results, as shown in Fig. 2.

In addition, it is presumed that $y_s \geq y_r$. Both, y_s and y_r imply a trade-off in between heat losses and pressure losses. Since the return temperature is always lower than the supply temperature in the DHN, it is of no use to have smaller return diameters than supply diameters.

3.5. Optimization algorithm

Genetic algorithms are a common class of optimization algorithms used for planning energy systems based on simulations. For instance, a DHN planning was performed using a genetic algorithm in [31], multistage expansion planning of an electric energy grid in [45], and energy quality management of buildings in [46]. However, in other engineering domains, such as aerospace systems, *surrogate algorithms* are often used to solve optimization problems based on simulations [47]. Furthermore, the results of [16] show that the objective of a DHN co-planning problem can be easily approximated by known functions, making it reasonable to use a surrogate approach. In conclusion, in this work, a surrogate optimization approach is chosen to find the optimal configuration of planning variables for the co-planning of a DHN. The *Matlab* surrogate optimization procedure is used due to its user-friendly documentation and implementation regarding parallelization, incorporation of the parameter study, and visual display of convergence. The *Matlab* surrogate algorithm incorporates various stopping criteria, such as a maximum number of function calls or running time. In this work, the objective is displayed after each iteration, and the user stops the optimization manually if the optimizer does not converge further.

4. Case study

The case study used to illustrate the DHN co-planning approach is located in Hamburg, Germany and consists of 80 houses, as shown in Fig. 3(a).

4.1. Finding the optimal topology

In Section 2.4, three different algorithms were presented for finding the optimal DHN topology. To compare the approaches, five different

Table 1
Metric values for each topology search algorithm used to find the optimal topology for the case study.

Algorithm	ℓ_Σ in km	ℓ_{cc} in km	t_{comp} in s	P_{pu} in kW	γ in %
Kou (*networkX*)	18.368	1.562	61.752	51.351	6.916
Shortest path	25.395	0.915	0.853	36.248	7.567
Constrained Steiner					
$\beta = 1$	23.081	0.915	108.478	31.213	7.344
$\beta = 1.25$	18.984	1.121	57.7	39.268	6.933
$\beta = 1.5$	17.865	1.315	44.668	41.282	6.833

metrics were selected. The first one is the overall piping length ℓ_Σ, determining the investment cost. The second metric, ℓ_{cc}, has a major influence on the operating costs of the DHN. In order to understand the influence of ℓ_{cc} on the operating costs, each optimal topology has to be simulated for one time step with $\dot{Q}^b_{max}$ for each building b as heating demand in order to calculate the required pumping power P_{pu} and the heat losses $\gamma = \frac{\dot{Q}^{max}_{gen} - \dot{Q}^{max}_{b}}{\dot{Q}^{max}_{gen}}$ with $\dot{Q}^{max}_{b} = \sum_{b\in\mathcal{B}} \dot{Q}^{max}_{b}$. The simulation is performed using *pandapipes* with the assumption $y_s = y_r = 150\,\mathrm{Pa\,m^{-1}}$. Starting with an initial pressure difference of $\Delta p_{gen} = 0.5$ bar, Δp_{gen} is iteratively increased by 0.1 bar until the pressure difference $p^s_b - p^r_b$ is positive at each consumer b, since no additional pressure difference is required anymore at the house stations. The resulting pressure difference Δp_{gen} together with the mass flow $\dot{m}_{gen}$ gives P_{pu}. To calculate γ, an initial supply temperature $T^s_{gen} = 60\,^\circ$C is selected. Again, T^s_{gen} is increased iteratively by 0.5 °C until no supply temperature at the return junction of any consumer is less than 50 °C. The resulting T^s_{gen} is used to calculate $\dot{Q}^{max}_{gen} = c_w \dot{m}_{gen}\left(T^s_{gen} - T^r_{gen}\right)$ with the return temperature T^r_{gen} at the generator. The two simulation results P_{pu} and γ are chosen as metrics. Furthermore, the computation time t_{comp} is selected as the last metric.

The metrics for each topology search algorithm are collected in Table 1. The resulting topologies of the search algorithms are shown in Fig. 3. Unexpectedly, Kou's algorithm implemented in *networkX* does not result in the lowest value for ℓ_Σ and therefore does not result in the optimal topology. This may be due to the implementation in *networkX*. Since ℓ_{cc} is not directly considered in the Steiner tree computation, the resulting ℓ_{cc} is the highest value. Also, t_{comp} is the second longest. To perform the first step of Kou's algorithm, the shortest path is calculated for each node combination in $\mathcal{G}_{rou}$. When the ratio of terminal nodes to the number of nodes in $\mathcal{G}_{rou}$ is high, this procedure is advantageous because special shortest path algorithms can be used. However, in the case of the DHN topology search, the share of terminal nodes is low. Therefore, the way Kou's algorithm is implemented in *networkX* is inefficient for this task.

Due to the simplicity of the topology search algorithm based on shortest path search, it took less than a second to find the optimal topology. Furthermore ℓ_{cc} takes the lowest possible value which is a direct result of the way the algorithm works, as explained in Appendix B.3. The simplicity comes with the major disadvantage that the total topology length $\ell_\Sigma\left(\mathcal{G}_{dhn}\right)$ is relatively large, as can be seen in Table 1. For the case study, the algorithm leads to a star-shaped topology (Fig. 3(b)) without any loops.

In the case of the constrained Steiner algorithm, for $\beta = 1$ and $\beta = 1.25$ the topology search results in a meshed topology. Although for $\beta = 1$ the topology is meshed and ℓ_{cc} takes the same value as for the shortest path based algorithm, ℓ_Σ is about 2.3 km lower. This is achieved by a significantly higher computation time. The algorithm is the slowest and took 108.478 s. However, the computation time decreases with increasing β. The algorithms for $\beta = 1.25$ and $\beta = 1.5$ are both faster than Kou's algorithm. Since β is a tuning factor that represent the trade-off between operational and investment costs, as β increases, ℓ_{cc} increases and ℓ_Σ decreases. Although the optimal topology is meshed for $\beta = 1.25$, ℓ_Σ is only 0.616 km longer than for Kou's algorithm. In the case of $\beta = 1.5$, ℓ_Σ is even 0.5 km shorter compared to the results of Kou's algorithm.

Analyzing the two metrics P_{pu} and γ, both of which have a major influence on the operating cost of the DHN, it is clear that P_{pu} decreases with ℓ_{cc} and γ decreases with ℓ_Σ.

4.2. Results of the parameter study

The results of the parameter study are displayed using three dimensional plots. If there are multiple z-axis values for a given combination of x- and y-axes values, the minimum value is chosen for the z-axis.

4.2.1. Without domestic hot water

Heat losses and pumping energy. The yearly heat losses

$$\gamma = \frac{\sum_{k\in\mathcal{K}} \dot{Q}_{gen}(k) - \sum_{b\in\mathcal{B}} \dot{Q}_b(k)}{\sum_{k\in\mathcal{K}} \dot{Q}_{gen}(k)} \tag{11}$$

resulting from the simulations of the parameter study are plotted in Fig. 4(a). As can be seen in Fig. 4(a), the supply temperature parameters u_0 and u_1 have a greater influence on γ than y_s and y_r. With an increasing y_s and an increasing y_r, γ decreases. Furthermore, γ decreases with u_0 and decreases with u_1 if $u_0 \geq 100\,^\circ$C. When $u_0 < 100\,^\circ$C, γ shows a parabolic behavior for different u_1 values. The minimum of γ is at $\left[70\,^\circ\mathrm{C} \quad -1 \quad 2000\,\mathrm{Pa\,m^{-1}} \quad 2000\,\mathrm{Pa\,m^{-1}}\right]$. Fig. 4(b) shows the yearly electrical energy of the pump $E_{pu} = \Delta t \sum_{k\in\mathcal{K}} P_{pu}(k)$. For $y_s \leq 1200\,\mathrm{Pa\,m^{-1}}$, E_{pu} increases quadratically with y_s. However, for $y_s > 1200\,\mathrm{Pa\,m^{-1}}$ the increase of E_{pu} is approximately linear. This is due to the fact that only distinct diameters are allowed. Hence, for $y_s > 1200\,\mathrm{Pa\,m^{-1}}$ the smallest pipe has already been selected for some pipes and therefore a further increase of y_s or y_r would have no influence on the diameter and therefore on E_{pu}. Since a lower T^s_{gen} results in a higher $\dot{m}_{gen}$, E_{pu} decreases with an increasing u_0. The maximum of E_{pu} is at $\left[70\,^\circ\mathrm{C} \quad 0 \quad 2000\,\mathrm{Pa\,m^{-1}} \quad 2000\,\mathrm{Pa\,m^{-1}}\right]$ and the minimum at $\left[110\,^\circ\mathrm{C} \quad 0 \quad 400\,\mathrm{Pa\,m^{-1}} \quad 200\,\mathrm{Pa\,m^{-1}}\right]$. When $u_0 = 70\,^\circ$C, E_{pu} increases with an increasing u_1, otherwise E_{pu} decreases with an increasing u_1.

In summary, if E_{pu} decreases, γ increases and vice versa and therefore have to be analyzed together. This is in line with the results from [38]. Furthermore, the optimal choice of u_1 heavily depends on the choice of u_0.

Objective. The yearly cost of the DHN depends not only on the supply temperature and the parameterization, but also on generation unit choice. For all three generator types, the objective J is shown in Fig. 5. In the case of the HP, the main influence on J is u_0, which is due to the COP. Compared to y_s, the influence of y_s on J is almost negligible. The smaller the choice of u_0, the closer the optimal u_1 is to 0. A more negative u_1 would lead to higher supply temperatures in case of negative outdoor temperatures. The optimal choice of design variables in the case of a HP is $\left[70\,^\circ\mathrm{C} \quad -1 \quad 800\,\mathrm{Pa\,m^{-1}} \quad 200\,\mathrm{Pa\,m^{-1}}\right]$ resulting in $J_{opt} = 0.359$ mil. € and $J_{inv} = 1.51$ mil. €.

In the case of the CHP, the influence of y_s on J is significant, as can be seen in Fig. 5(b). The optimal design variable configuration in the case of the CHP is $\left[70\,^\circ\mathrm{C} \quad -2 \quad 2000\,\mathrm{Pa\,m^{-1}} \quad 600\,\mathrm{Pa\,m^{-1}}\right]$, resulting in $J_{opt} = 0.86$ mil. € and $J_{inv} = 1.146$ mil. €. Again, the lowest value for J is obtained by choosing the lowest possible value for u_0. However, a higher dependence on the outdoor temperature, i. e. a more negative u_1, is chosen compared to the HP, since there is no influence of T^s_{gen} on the efficiency of the CHP. Compared to the HP, the optimum pipe diameter is significantly reduced.

In the case of serial connection of a HP and a CHP, the optimal design variable configuration is $\left[70\,^\circ\mathrm{C} \quad 0 \quad 800\,\mathrm{Pa\,m^{-1}} \quad 200\,\mathrm{Pa\,m^{-1}}\right]$, resulting in $J_{opt} = 0.357$ mil. € and $J_{inv} = 1.64$ mil. €. Thus, the serial connection has the lowest operating cost, but due to the high investment cost, the annual cost J is higher than for the HP (Fig. 5(c)). Unlike the cost in case of a single HP or a single CHP, J is less continuous. This is due to the investment cost of the CHP. For example, in the case of

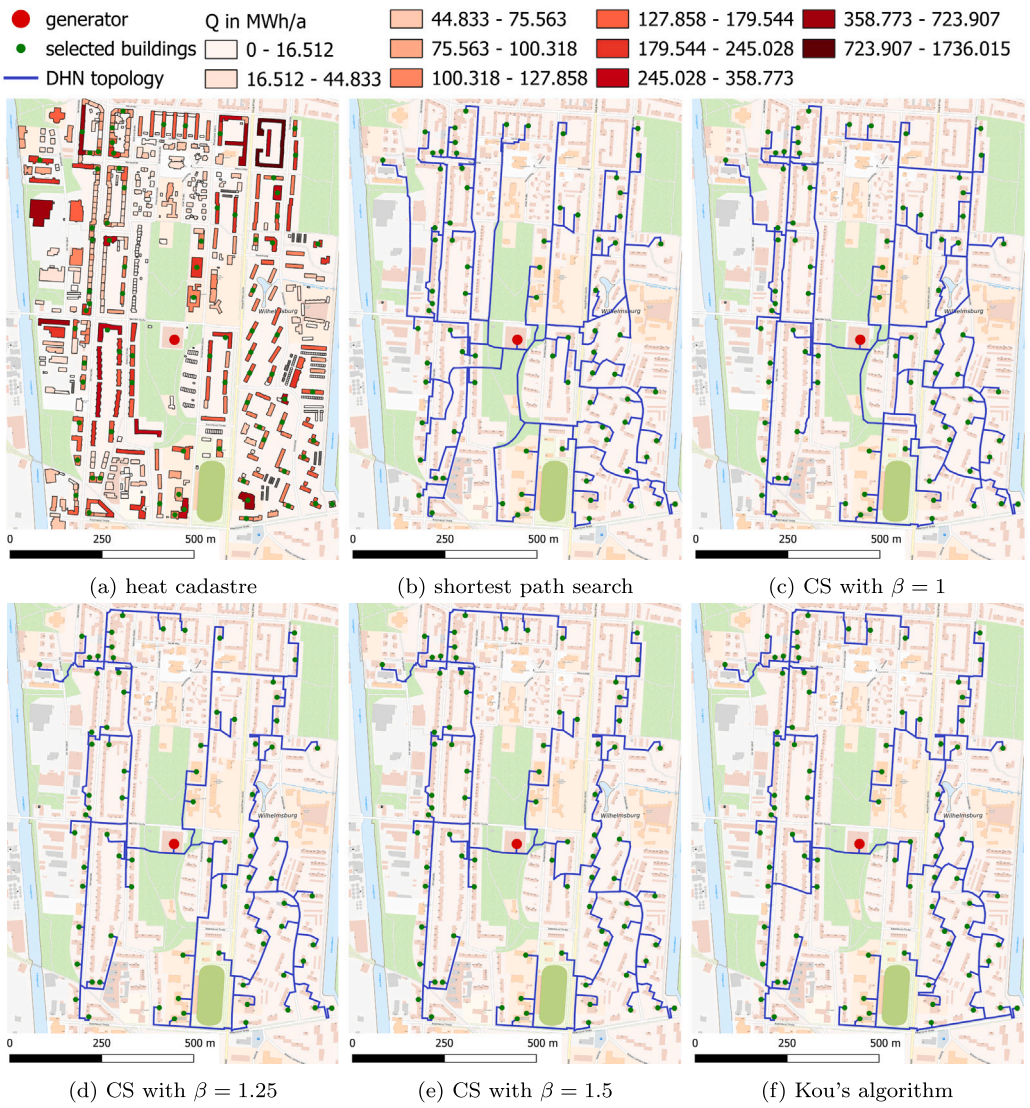

(a) heat cadastre (b) shortest path search (c) CS with $\beta = 1$

(d) CS with $\beta = 1.25$ (e) CS with $\beta = 1.5$ (f) Kou's algorithm

Fig. 3. Results of the topology optimization, including three different β parameters for the constrained Steiner (CS) algorithm.

$[70\,°\text{C} \quad 0 \quad 800\,\text{Pa}\,\text{m}^{-1} \quad 200\,\text{Pa}\,\text{m}^{-1}]$, the maximum required heating power of the CHP is $\dot{Q}_{\text{chp}}^{\text{max}} = 5.0254\,\text{MW}$, resulting in an annualized cost for the CHP of 0.135 mil. €. In the case of the design variable configuration $[70\,°\text{C} \quad -1 \quad 800\,\text{Pa}\,\text{m}^{-1} \quad 200\,\text{Pa}\,\text{m}^{-1}]$, the maximum required heating power of the CHP is $\dot{Q}_{\text{chp}}^{\text{max}} = 5.21\,\text{MW}$, resulting in an annualized cost for the CHP of 0.247 mil. €, since a larger CHP is required (see the CHP data in Table C.5).

4.2.2. With domestic hot water

Heat losses and pumping energy. In the case where the DHW demand is supplied by the DHN, the heat losses of the DHN are significantly higher. The minimum of γ is 8.748% compared to 4.459% when the DHW demand is not supplied by the DHN (Fig. 6(a) compared to Fig. 4(a)). The same applies to the electrical energy required by the pump (see Fig. 6(b) compared to Fig. 4(b)). The increased values for γ and P_{pu} result from additional mass flow peaks due to the DHW demand, as can be seen in Fig. 7. Fig. 7 shows the mass flow $\dot{m}_{\text{gen}}$ for one week in March, with a peak on the morning of March 7. Fig. 7 also shows the mass flow $\dot{m}_{\text{b}}$ through the house station and the DHW storage tank temperature T_{dhw} of the building with the highest DHW demand. As can be seen, T_{dhw} is about 42 °C when the morning DHW demand peak begins. Therefore, the DHN must meet the entire DHW peak due to the low storage temperature. If the storage temperature is low in several house stations at the same time when a DHW load peak occurs, $\dot{m}_{\text{gen}}$ is suddenly increased, resulting in a higher pumping demand.

Objective. In the case of DHW supply by DHN, the objective values resulting from the parameter study for all three generation unit options are shown in Fig. 8. For HP and CHP, the trend of the objective is similar to the one without DHW supply by DHN (Fig. 8 compared to Fig. 5). However, there is a difference between the two trends, since the DHW supply by the DHN results in a higher heating demand, which leads to higher objective. In the case of the CHP, the difference is approximately 0.1 mil. € and in the case of the HP, approximately 0.03 mil. €. In the case of the serial generation unit, the objective is more continuous compared to the objective without DHW supply, since all simulations of the parameter study result in the same CHP and HP sizes.

4.3. Optimal DHN configuration

The results of the parameter study are used as a starting point for a *surrogate* optimization. All design variables are assumed to be integers. The design variable u_0 is bounded by 70 °C and 100 °C and the resolution is 0.5 °C, the resolution of u_1 is 0.05 with lower and upper

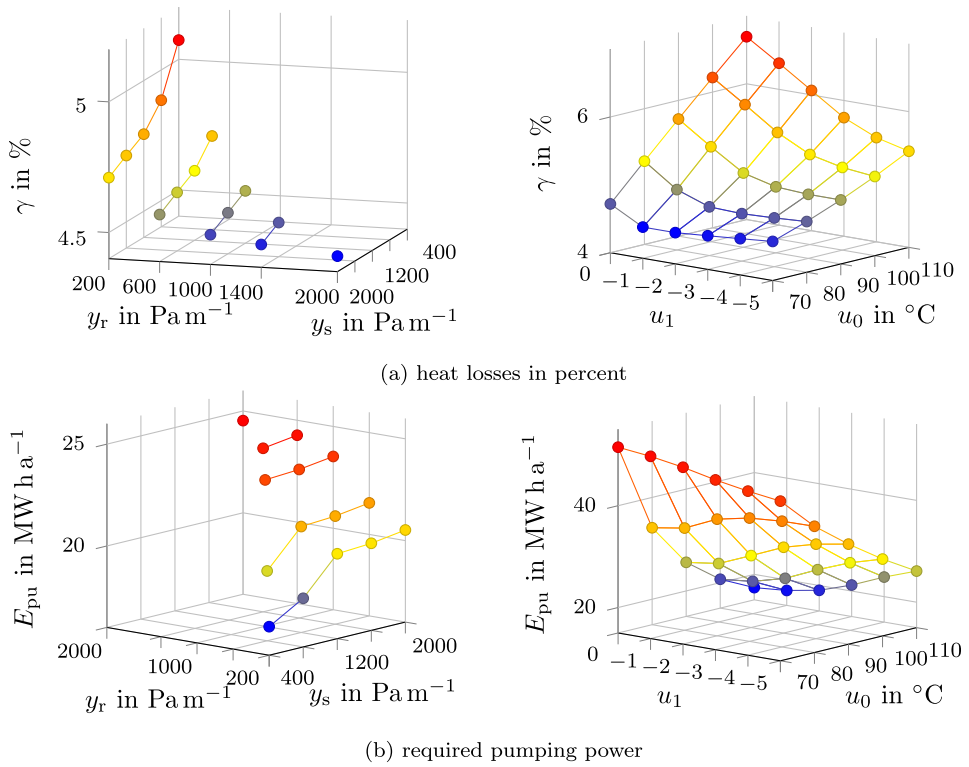

Fig. 4. Heat losses and required pumping power for each design value configuration of the parameter study if DHW is not supplied by the DHN.

bounds of −5 and 0. For the TPLs, a resolution of 100 Pa m^{-1} is chosen, with a lower bound of 200 Pa m^{-1} and an upper bound of 2000 Pa m^{-1}, based on the results of [38].

4.3.1. Without domestic hot water

In case DHW is not supplied by the DHN, the optimal design variable configuration is $\lceil 70\,°C \quad -1.1 \quad 800\,Pa\,m^{-1} \quad 200\,Pa\,m^{-1} \quad hp \rfloor$ with $J_{opt} = 0.359$ mil. € and $J_{inv} = 1.505$ mil. €. The annual cost J for the optimal HP system is 0.143 mil. € lower than for the optimal CHP system and 0.133 mil. € lower than for the serial system, although the serial system has the lowest operating cost.

The heating power of the CHP and the HP for each time step in the case of the optimal serial DHN configuration is shown in Fig. 9 for July and December. In July, the CHP is not used, due to relatively low electricity prices and high COPs. However, in December, the maximum heating power of both generators is almost equal.

4.3.2. With domestic hot water

If DHW is supplied by the DHN, the optimal design variable configuration is $\lceil 70\,°C \quad -0.6 \quad 1700\,Pa\,m^{-1} \quad 500\,Pa\,m^{-1} \quad hp \rfloor$ with $J = 1.921$ mil. €. The optimal u_1 is lower compared to the optimal u_1 if DHW is not supplied by the DHN. This means that the supply temperature is less dependent on the outdoor temperature, resulting in higher temperatures in the summer months compared to the case without DHW supply by the DHN. This is a result of the higher summer heating demand due to the DHW demand. The diameters are significantly smaller when the DHW demand is supplied by the DHN. However, the diameters do not have a significant effect on J as can be seen in Fig. 8(a). The optimal generation unit is a HP. The minimum annualized investment cost is 0.19 mil. € cheaper than the CHP case and 0.239 mil. € cheaper than the serial generation unit case.

4.3.3. Optimal DHW configuration

According to the optimization results, the HP is the optimal generation unit for the specific DHN with the specific cost data. In order to compare the two configurations, the one with DHW supply by the DHN and the one without DHW supply by the DHN, the cost of DHW supply by electric boilers must first be calculated. The annual DHW demand of the DHN is 1288 MW h. Using the time-dependent electricity price (average electricity price of 44.487 € MW^{-1} h^{-1}) and an assumed efficiency of 0.95, the result is 0.0603 mil. €. Additional investment costs are not considered because electric boilers are usually cheap and it is assumed that they do not significantly change the investment cost of the house station.

Adding the cost of DHW supply with electric boilers to the annualized cost of the DHN results in an annualized cost of 1.924 mil. €. Compared to $J = 1.921$ mil. € when DHW is supplied by the DHN, it is cheaper to supply the DHW demand with the DHN, although the difference is marginal.

4.4. Sensitivity analysis

Uncertainty in energy systems is a fact that should not be underestimated. Therefore, as a final step in the co-planning process, a sensitivity analysis of the CO_2 price c_{CO_2} is performed. For the sensitivity analysis, c_{CO_2} is varied, resulting in a variation of the gas price (see (9)). For each value $c_{CO_2} \in \{55\,€\,t^{-1}, 81.275\,€\,t^{-1}, 107.55\,€\,t^{-1}, 133.825\,€\,t^{-1}\}$ and for each design variable configuration $\boldsymbol{z}$ that has already been simulated, J is calculated. For each generation unit type and each c_{CO_2}, the lowest J is selected, resulting in Fig. 10.

Assuming linear interpolation between discrete CO_2 prices, a CHP is the best choice for $c_{CO_2} \leq 84.72\,€\,t^{-1}$. For $c_{CO_2} > 84.72\,€\,t^{-1}$, a HP is the optimal choice. A serial combination of both generator types is never optimal because of the higher investment costs. As Fig. 10 shows, there is no increase in J when c_{CO_2} is increased from $107.55\,€\,t^{-1}$ to $133.825\,€\,t^{-1}$ in the case of the serial connection. Therefore, the CHP of the serial connection is not utilized for $c_{CO_2} \geq 107.55\,€\,t^{-1}$. However, a serial DHN may be the optimal choice for DHNs with a higher peak demand.

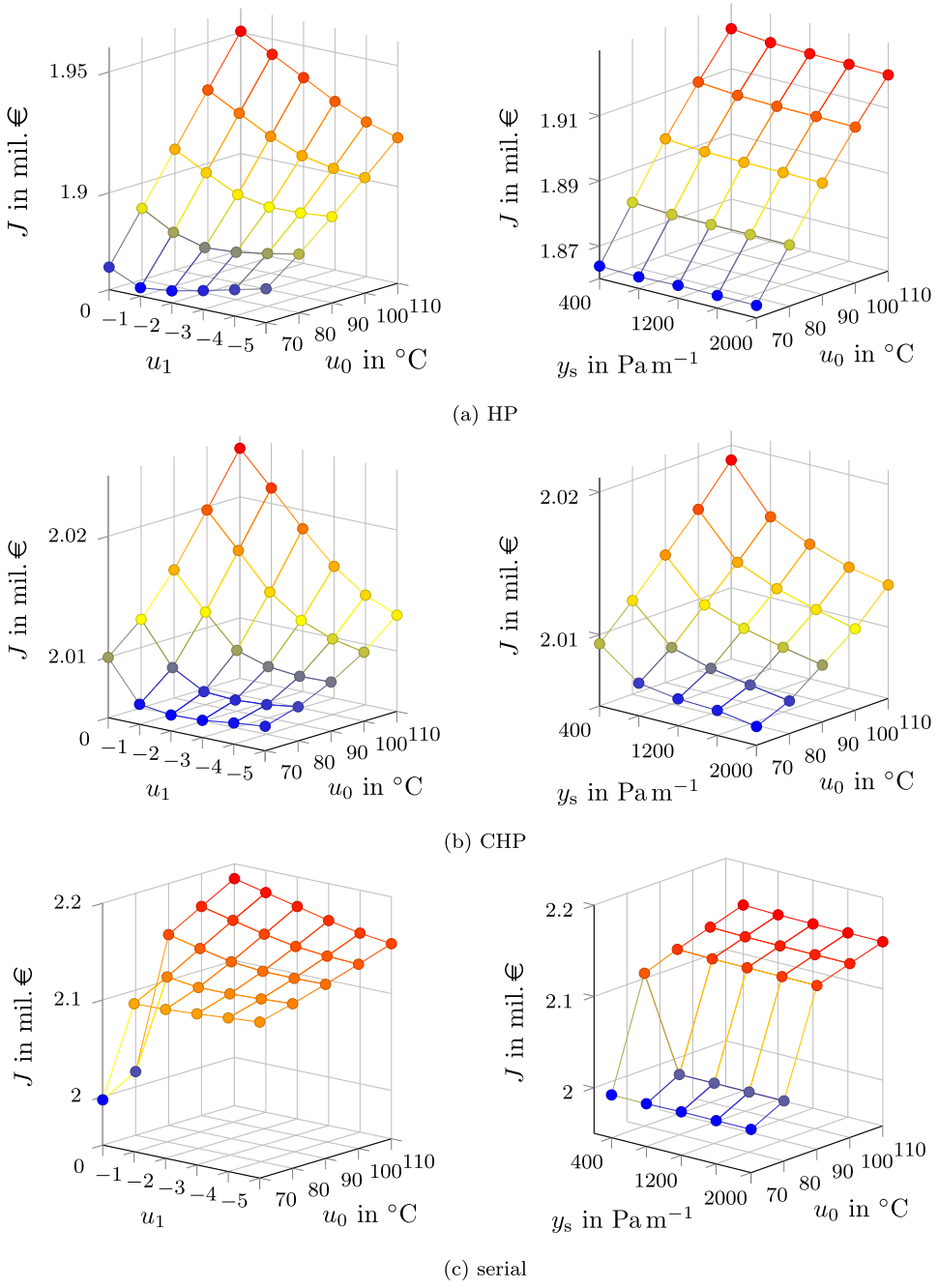

(a) HP

(b) CHP

(c) serial

Fig. 5. Objective value for all three generator types of the parameter study if DHW is not supplied by the DHN.

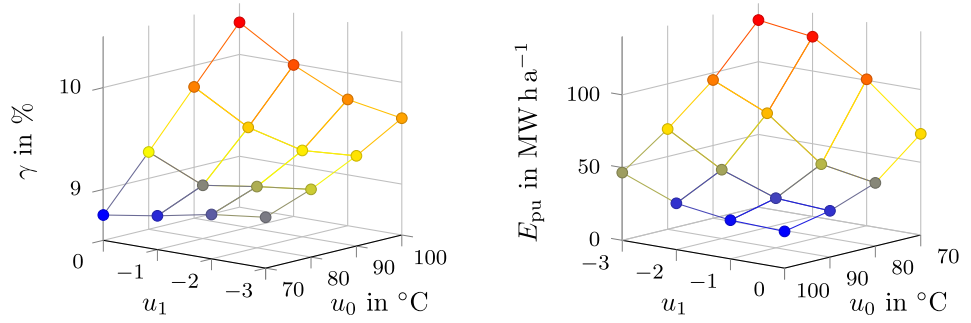

(a) heat losses

(b) required pumping power

Fig. 6. Heat losses and required pumping power for each design value configuration of the parameter study in the case DHW is supplied by the DHN.

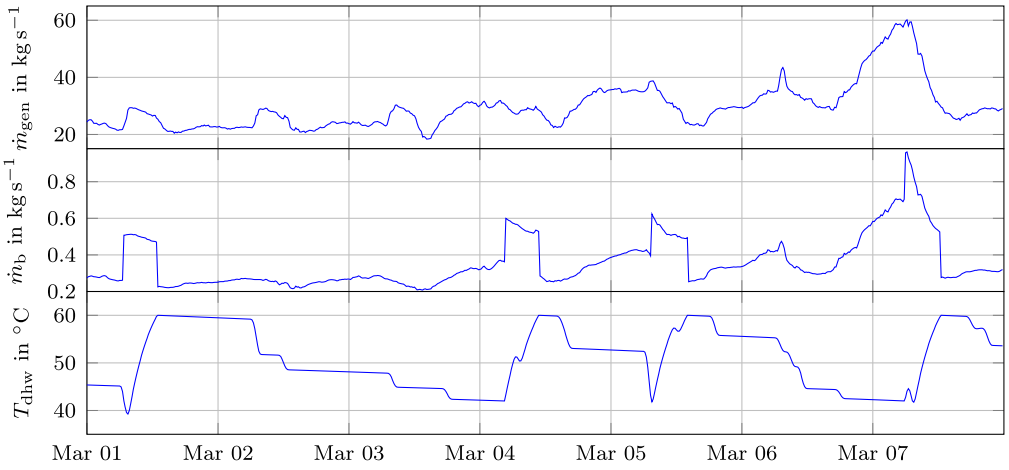

Fig. 7. Mass flow $\dot{m}_{gen}$ of generation unit, mass flow $\dot{m}_b$ of building with highest DHW demand, and DHW storage tank temperature T_{dhw} of building with highest DHW demand for $y_s = 1200\,\mathrm{Pa\,m^{-1}}$, $y_r = 600\,\mathrm{Pa\,m^{-1}}$, $u_0 = 70\,°\mathrm{C}$, and $u_1 = 0$.

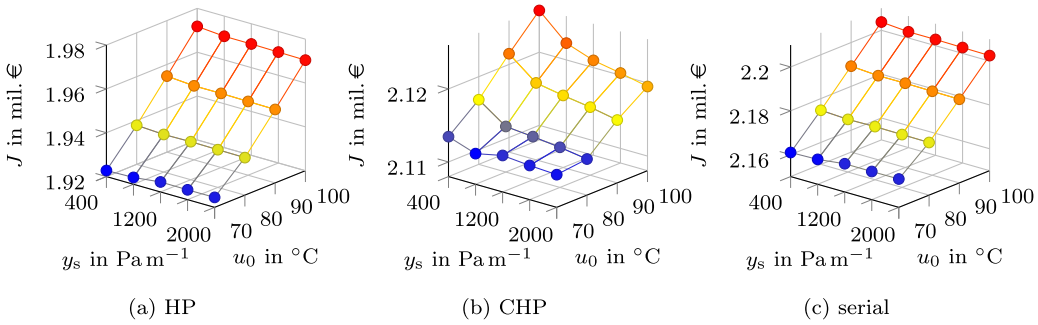

Fig. 8. Objective value for all three generator types of the parameter study in the case DHW is supplied by the DHN.

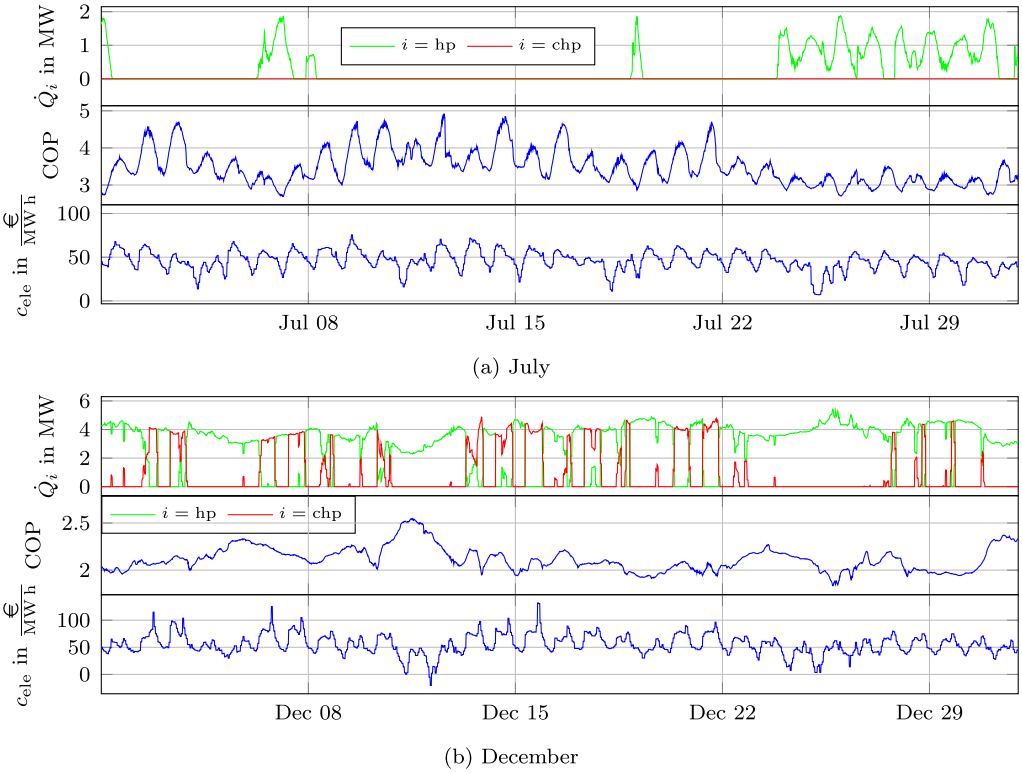

Fig. 9. Heating power of HP and CHP, COP, and electricity price for $y_s = 800\,\mathrm{Pa\,m^{-1}}$, $y_r = 200\,\mathrm{Pa\,m^{-1}}$, $u_0 = 70\,°\mathrm{C}$, and $u_1 = 0$ if DHW is not supplied by the DHN.

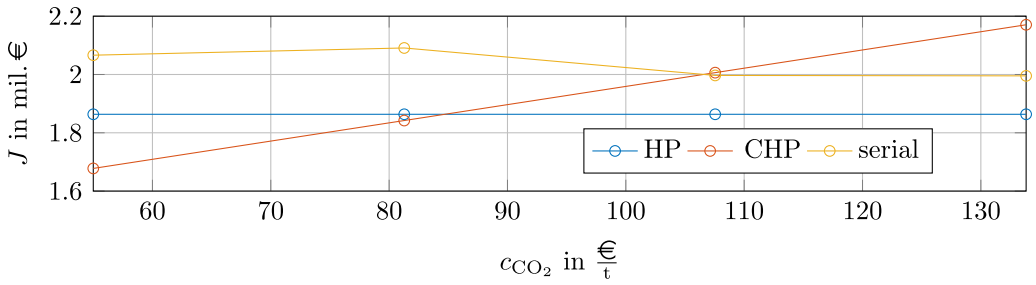

Fig. 10. Sensitivity analysis for all three generation units regarding the CO_2 price.

4.5. Simulation time

Each full-year dynamic simulation without the DHW model took between 13 min and 14 min. Since there is no limit to parallelization, the approach is scalable. Additionally, the simulation results can be reused for a sensitivity analysis. When DHW was supplied by the DHN, the simulation took between three and four hours, mainly due to the control of the DHW storage tanks. Therefore, a simpler control strategy than a bang–bang controller may be more appropriate in terms of simulation time. However, as described in Section 4.2.2, DHW control affects the optimization results.

5. Conclusion

This work presents a novel two-step co-planning approach for district heating networks. In a first step, a new algorithm for finding the optimal topology from a set of possible routes is presented and compared with approaches from the literature. This comparison shows that the *constrained Steiner tree algorithm* presented in this work outperforms the other approaches. Furthermore, the algorithm introduces a parameter β, for balancing the objectives of minimum piping length and minimum distance to the critical consumer. Next, a dynamic simulation model is automatically generated from the topology, where the diameters of the pipes are parameterized based on target pressure losses.

In a second step, the simulation is run within a surrogate optimization loop to find the optimal DHN configuration. The target pressure losses, together with the supply temperature parameters and a choice of generating unit, define the set of design variables. The results of the optimization show that whether a combined heat and power unit or a heat pump is the better choice as a generating unit depends on the CO_2 price. At the current CO_2 price for Germany of 55 €t^{-1}, a combined heat and power unit is the optimal choice. However, for CO_2 prices higher than 84.72 €t^{-1}, a heat pump is the optimal choice. Due to the high investment costs, the serial generation unit consisting of both types is never the optimal choice. However, for district heating networks with higher peak demand, a serial generating unit may be more appropriate.

For the district heating network with a single gas-fueled combined heat and power unit, the smallest possible diameters are selected due to the higher supply temperatures compared to a network with heat pump. In the case of the district heating network with a single heat pump, the supply temperature parameters are the main influence on the operating costs. Due to the lower maximum supply temperatures, pipe diameters are less important in comparison with the combined heat and power unit case. Furthermore, smaller supply diameters than return diameters are reasonable for all generating units.

CRediT authorship contribution statement

Jonathan Vieth: Writing – original draft, Validation, Software, Resources, Project administration, Methodology, Conceptualization. **Jan Westphal:** Writing – review & editing, Validation, Software. **Arne Speerforck:** Writing – review & editing, Supervision, Funding acquisition.

Declaration of Generative AI and AI-assisted technologies in the writing process

During the preparation of this work, the authors used DeepL Write in order to improve language and readability. After using this tool, the authors reviewed and edited the content as needed and take full responsibility for the content of the published article.

Declaration of competing interest

The authors declare that they have no known competing financial interests or personal relationships that could have appeared to influence the work reported in this paper.

Acknowledgment

This research is supported by the German federal ministry of economic affairs and climate action (BMWK) under the agreement no. 03EWR007O2.

Appendix A. Automated simulation model generation

A.1. Topology optimization algorithms

In this work, three different algorithms for finding the optimal topology are compared. The first algorithm is the Steiner tree algorithm presented in [14] and therefore not explained in this work. The second algorithm [12] was developed for DHNs and is based on shortest path search. The corresponding algorithm is explained in Algorithm 1. In this work, a newly developed algorithm is presented incorporating the DHN operation into the topology search. This algorithm is explained in detail in Algorithm 2.

A.2. Model parameterization

A DHN consists of supply pipes and return pipes. Therefore, each $e \in \mathcal{E}_{\text{dhn}}$ is represented by a supply pipe $s \in \mathcal{E}_{\text{s}}$ and a return pipe $r \in \mathcal{E}_{\text{r}}$ in the graph $\mathcal{G}_{\text{sim}} = (\mathcal{N}_{\text{sim}}, \mathcal{E}_{\text{sim}})$, where $\mathcal{E}_{\text{s}}$ is the set of supply pipes and $\mathcal{E}_{\text{r}}$ is the set of return pipes. Furthermore, in contrast to $\mathcal{G}_{\text{dhn}}$ consumers and producers in $\mathcal{G}_{\text{sim}}$ are modeled by edges connecting the supply and return pipes, as is often done when simulating DHNs [48]. To run simulations, for each pipe $p \in \mathcal{E}_{\text{s}} \cup \mathcal{E}_{\text{r}}$ a length ℓ_p, a diameter d_p, a heat loss factor U_p, and a pipe roughness ϵ_p have to be derived. The pipe roughness $\epsilon_p = \epsilon = 0.07$ mm is assumed to be constant in all pipes and ℓ_p is known from $\ell(e)$, where e is the edge in $\mathcal{E}_{\text{dhn}}$ corresponding to p.

To dimension the pipe diameters, a maximum mass flow $\dot{m}^p_{\max}$ must be calculated for each pipe p based on the consumer demands. Assuming a constant temperature difference $\Delta T = T_{\text{s}} - T_{\text{r}} = 30$ K in between the supply temperature T_{s} and the return temperature T_{r} at each consumer the maximum required mass flow $\dot{m}^b_{\max} = \frac{\dot{Q}^b_{\max}}{c_{\text{w}} \Delta T}$ can be calculated assuming a constant heat capacity of water $c_{\text{w}} =$

Algorithm 1 Optimal topology by shortest path search

$\mathcal{E}_{\text{dhn}} \leftarrow$ empty set
for $n \in \mathcal{N}_{\text{b}}$ **do**
  $\mathcal{E}_n \leftarrow$ shortest path from g to n
  for $e \in \mathcal{E}_n$ **do**
    if $e \notin \mathcal{E}_{\text{dhn}}$ **then**
      add e to $\mathcal{E}_{\text{dhn}}$
    end if
  end for
end for

Algorithm 2 Optimal topology by constrained Steiner tree

$\mathcal{E}_{\text{dhn}} \leftarrow$ empty set, $\mathcal{N}_{\text{dhn}} \leftarrow \{g\}$ ▷ Initialize graph $\mathcal{G}_{\text{dhn}}$ with generator node g
$c(e) \leftarrow \ell(e), \quad \forall e \in \mathcal{E}_{\text{rou}}$ ▷ create a copy of the distance
$\overline{\mathcal{N}}_{\text{dhn}} \leftarrow \mathcal{N}_{\text{b}}$ ▷ set of unprocessed nodes
for $n \in \mathcal{N}_{\text{b}}$ **do** ▷ Calculate shortest path and length from g to all building nodes
  $\mathcal{E}_n \leftarrow \text{sp}\left(\mathcal{G}_{\text{rou}}, g, n, \ell\right)$
  $\ell_n \leftarrow \sum_{e\in\mathcal{E}_n} \ell(e)$
end for
$\ell_{\max} \leftarrow \beta \max\{\ell_1, \ell_2, \ldots, \ell_{|\mathcal{N}_{\text{b}}|}\}$ ▷ maximum distance from g to any consumer
while $\overline{\mathcal{N}}_{\text{dhn}}$ is not empty **do** ▷ connect all buildings iteratively to $\mathcal{G}_{\text{dhn}}$
  $p \leftarrow \infty$
  for $r \in \overline{\mathcal{N}}_{\text{dhn}}$ **do**
    $\mathcal{E}_r \leftarrow \text{sp}\left(\mathcal{G}_{\text{rou}}, \mathcal{N}_{\text{dhn}}, r, \ell\right)$
    if $\sum_{e\in\mathcal{E}_r} \ell(e) \le p$ **then**
      $\hat{\mathcal{G}}_{\text{dhn}} \leftarrow \mathcal{G}_{\text{dhn}}$ with nodes and edges from $\mathcal{E}_r$
      $\hat{\mathcal{E}}_r \leftarrow \text{sp}\left(\hat{\mathcal{G}}, g, r, \ell\right)$
      if $\sum_{e\in\hat{\mathcal{E}}_r} \ell(e) \le \ell_{\max}$ **then** ▷ check if $\mathcal{E}_r$ violates (2e)
        $\mathcal{E}_{\text{sp}} \leftarrow \mathcal{E}_r$
        $p \leftarrow \sum_{e\in\mathcal{E}_{\text{sp}}} \ell(e)$
      end if
    end if
  end for
  if p is ∞ **then** ▷ If not shortest path satisfies (3)
    $\epsilon \leftarrow \Delta\epsilon$
    while $p > \ell_{\max}$ **do**
      $w(e) \leftarrow \epsilon\ell(e) + (1-\epsilon)c(e), \quad \forall e \in \mathcal{E}_{\text{rou}}$ ▷ weighted sum of cost and distance
      $\mathcal{E}_r, r \leftarrow \text{msp}\left(\mathcal{G}_{\text{rou}}, \mathcal{N}_{\text{dhn}}, g, w\right)$
      $\hat{\mathcal{G}} \leftarrow \mathcal{G}_{\text{dhn}}$ with nodes and edges from $\mathcal{E}_r$
      $\hat{\mathcal{E}}_r \leftarrow \text{sp}\left(\hat{\mathcal{G}}, g, r, \ell\right)$
      $p \leftarrow \sum_{e\in\hat{\mathcal{E}}_r} \ell(e)$
      $\epsilon \leftarrow \epsilon + \Delta\epsilon$
    end while
    $\mathcal{E}_{\text{sp}} \leftarrow \mathcal{E}_r$
  end if
  add all edges and nodes from $\mathcal{E}_{\text{sp}}$ to $\mathcal{G}_{\text{dhn}}$
  $c(e) \leftarrow 0, \quad \forall e \in \mathcal{E}_{\text{sp}}$ ▷ set cost to zero for all added edges
  remove r from $\overline{\mathcal{N}}_{\text{dhn}}$
end while

$4186\,\text{J}\,\text{kg}^{-1}\,\text{K}^{-1}$ and neglecting pressure losses. If $\mathcal{G}_{\text{dhn}}$ is a tree, for each p $\dot{m}^p_{\max}$ follows directly from $\dot{m}^b_{\max}$. If Algorithm 1 or Algorithm 2 is used to generate $\mathcal{G}_{\text{dhn}}$, $\mathcal{G}_{\text{dhn}}$ is not guaranteed to be a tree, i. e. the topology might contain a loop. If $\mathcal{G}_{\text{dhn}}$ is not a tree, a simulation of the DHN has to be performed using an initial diameter $d_0 = 1\,\text{m}$ in order to calculate $\dot{m}^p_{\max}$ for each p. The simulation of one time-step is performed in *pandapipes* [34]. At the generator, the supply temperature is fixed at $T^{\text{s}}_g = 80\,°\text{C}$. The resulting mass flow $\dot{m}^p_{\max}$ is not guaranteed to be the actual maximum mass flow, since other load conditions may result in higher mass flows in individual pipes. However, it is a good enough estimate.

As shown in Fig. 1, the target pressure loss (TPL) of the supply pipes y_{s} and the return pipes y_{r} are inputs to the DHN planning. A TPL describes the pressure loss per unit length of a pipe in the maximum load case [38]. Therefore, one design variable is obtained for all supply pipes and one design variable is obtained for all return pipes. From the TPL values, the maximum pressure loss in pipe $p \in \mathcal{E}_i$ is given by

$$\Delta p^p_{\max} = \ell_p y_i \tag{A.1a}$$

with $i \in \{\text{s}, \text{r}\}$. For linking $\Delta p^p_{\max}$ with $\dot{m}^p_{\max}$, the mass flow pressure loss correlation

$$\Delta p_p = -\frac{8\lambda_j(\dot{m}^p_{\max})\ell_p}{\rho\pi^2 d_p^5}\left(\dot{m}^p_{\max}\right)^2 \tag{A.1b}$$

is used, with the constant water density $\rho = 983.19\,\text{kg}\,\text{m}^{-3}$ and the friction factor correlation by Zanke [49]

$$\lambda = \left[-2\log\left(2.7\frac{\left[\log(\frac{4}{\pi\nu d_p}\dot{m}^p_{\max})\right]^{1.2}}{\frac{4}{\pi\nu d_p}\dot{m}^p_{\max}} + \frac{\epsilon}{3.71 d_p}\right)\right]^{-2}, \tag{A.1c}$$

which is valid for turbulent flows. The dynamic viscosity is assumed to be constant with $\nu = 4661 \times 10^{-6}\,\text{kg}\,\text{m}^{-1}\,\text{s}^{-1}$. By solving the system of Eqs. (A.1), an ideal diameter $\tilde{d}_p$ can be calculated for each pipe p. Since usually only DHN pipes with fixed diameters are available, the diameter d_p closest to $\tilde{d}_p$ can be selected from a catalog, as well as the matching U_p. The used pipe catalog is depicted in Table C.2.

Appendix B. Dynamic simulation model

The fluid circulating in the DHN is water with the constant fluid parameters ρ and c_{w}. The models of the DHN components used in the simulations are described below. The pipe model in Appendix B.1 and the junction model in Appendix B.2 are based on [43].

B.1. Pipe

The hydraulics of each pipe are modeled by the steady-state mass balance $\dot{m}_{\text{in}} + \dot{m}_{\text{out}} = 0$, with $\dot{m}_{\text{in}}$ the mass flow entering the pipe and $\dot{m}_{\text{out}}$ the mass flow leaving the pipe and the pressure loss given by (A.1b).

For the energy balance, each pipe is discretized by $n_{\text{cv}} = \max\{\lceil\ell\zeta\rfloor, 3\}$ control volumes (CVs), where $\zeta = 50\,\text{km}^{-1}$ is the number of CVs per pipe length. The operator $\lceil x \rfloor$ rounds x to the next closest integer. The dynamic energy balance within each CV is given by

$$\rho\frac{V_{\text{pi}}}{n_{\text{cv}}}\frac{\text{d}h_{\text{pi}}}{\text{d}t} = \dot{m}_{\text{in}}h_{\text{in}} - \dot{m}_{\text{in}}h_{\text{out}} - \dot{\hat{Q}}_{\text{pi}}, \tag{B.1}$$

where V_{pi} is the pipe internal volume, h_{in} is the specific enthalpy of the mass flow entering the CV, h_{out} is the specific enthalpy of the mass flow leaving the CV, and h_{pi} is the specific enthalpy of the water in the CV. The heat losses in each CV are given by

$$\dot{\hat{Q}}_{\text{pi}} = U\frac{\ell}{n_{\text{cv}}}\left(\frac{h_{\text{pi}}}{c_{\text{w}}} - T_{\text{so}}\right), \tag{B.2}$$

where T_{so} is the time-dependent soil temperature in °C.

B.2. Junction

In accordance with the pipe model, the dynamic energy balance

$$\rho V_{\text{ju}}\frac{\text{d}h_{\text{ju}}}{\text{d}t} = \sum_{e\in\mathcal{E}_{\text{ju}}}\dot{m}_e h_e \tag{B.3}$$

is used to model the thermal behavior of each junction. The set of edges $\mathcal{E}_{\text{ju}}$ are the edges connected to the junction with $\dot{m}_e$ and h_e is the mass flow of edge e and the specific enthalpy. $V_{\text{ju}} = 1\,\text{m}^3$ is the volume of each junction, and h_{ju} is the specific enthalpy of the water stored in the junction.

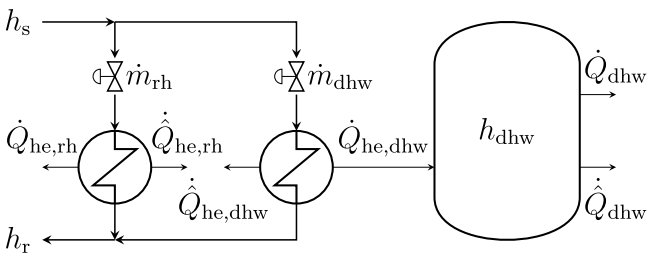

Fig. B.11. House station with hot water supply based on [50].

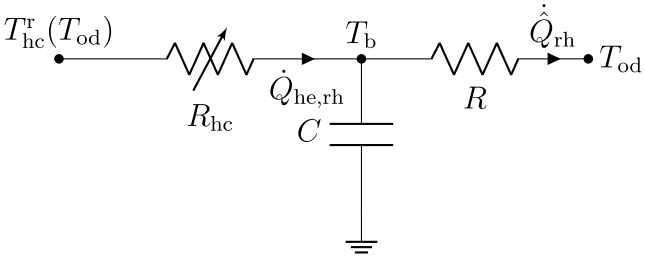

Fig. B.12. Building model represented as an electric equivalent circuit.

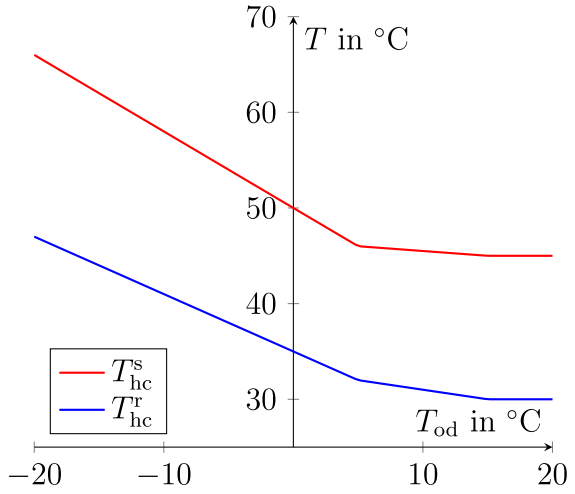

Fig. B.13. Radiator system control curves based on [50].

B.3. Consumers

One contribution of this work is to analyze the influence of DHW demand on the optimal design of a DHN. For this purpose, a consumer model is needed that includes the DHW demand and a hot water storage tank. The model used is based on [50] and depicted in Fig. B.11. The consumer model consists of a house station model, a building model, and a DHW model. The house station model is connected to the DHW model and the building model by two heat exchangers. All three models are described below.

B.3.1. House station model

Each valve in the house station model controls the mass flow through the following heat exchanger. The valve controlling the mass flow $\dot{m}_{rh}$ through the heat exchanger feeding the building is controlled by the indoor temperature of the building as explained in Appendix B.3.2, and the mass flow $\dot{m}_{dhw}$ through the heat exchanger feeding the hot water tank is controlled by the temperature of the hot water tank as explained in Appendix B.3.3. No pressure losses are considered other than the pressure loss in the valve.

The heat $\dot{Q}_{he,j}$ extracted from the DHN by the heat exchanger is calculated by

$$\dot{Q}_{he,j} = \dot{m}_j \left(h_s - h_r\right) - \dot{\hat{Q}}_{he,j} \tag{B.4}$$

with $j \in \{rh, dhw\}$ and the specific enthalpies h_s and h_r at the supply side and the return junction of the house station, respectively. The heat loss $\dot{\hat{Q}}_{he,j}$ is modeled by

$$\dot{\hat{Q}}_{he,j} = \dot{Q}_{he,j}\eta_{hs}\frac{T_s}{\hat{T}} \tag{B.5}$$

with $T_s = {}^{h_s}/_{c_w} + 273.15\,\mathrm{K}$ and the constant parameters $\eta_{hs} = 0.05$ and $\hat{T} = 373.15\,\mathrm{K}$. The parameters are chosen based on the data given in [51] that 5 % heat losses occur in house stations. However, the losses do depend on the supply temperature. Therefore, in (B.5), we assume that the heat losses are 5 % of the heat demand when $T_s = \hat{T}$.

B.3.2. Building model

An RC model is used to model each building. An electrical equivalent circuit of the building model is shown in Fig. B.12. The mass flow $\dot{m}_{rh}$ is controlled by a PI-controller with the goal of keeping the building temperature T_b close to the set temperature $T_{set} = 21\,^\circ\mathrm{C}$. The mass flow $\dot{m}_{rh}$ affects the heat $\dot{Q}_{he,rh}$ entering the heating system of the building.

Typically, the supply temperature T^s_{hc} within the radiator system of a building is controlled by an outdoor temperature dependent control curve [50]. It is assumed, that the return temperature T^r_{hc} of the radiator system is 15 °C–20 °C lower than T^s_{hc}. Both curves are depicted in Fig. B.13. The radiator temperature determines the required DHN temperature because heat transfer is not possible if the return temperature $T_r = {}^{h_r}/_{c_w} + 273.15\,\mathrm{K}$ is too low for the radiator system. Based on [43], the heat $\dot{Q}_b$ transferred to the building is calculated as

$$\dot{Q}_b = \dot{Q}_{max}\left(\frac{T_r - T^r_{hc}}{\Delta T_{nom}}\right)^n \tag{B.6}$$

where $\Delta T_{nom} = 8\,^\circ\mathrm{C}$ and $n = 1.33$.

The building itself is modeled by a heat capacity $C_b = c_{eff}A_b$ with an effective heat capacity $c_{eff} = 90\,\mathrm{W\,h\,m^{-2}\,K^{-1}}$ and a net building area A_b. The interaction with the environment is modeled by a thermal conductivity

$$G_b = \frac{1}{R_b} = \frac{Q_b}{24\,\mathrm{h}\sum_{d=1}^{365}\begin{cases} T_{set} - T_{od}(d), & T_{od}(d) \le 16\,^\circ\mathrm{C}, \\ 0, & \text{otherwise}, \end{cases}} \tag{B.7}$$

assuming that the heating system is not used above average daily outdoor temperatures of 16 °C. All required data, apart from T_{od}, can be taken from the heat cadastre.

B.3.3. Domestic hot water demand

If DHW demand is supplied by the DHN, a storage tank is required to lower the peak heat demand. A schematic drawing of the house station including the DHW demand is shown in Fig. B.11.

The hot water storage tank with volume V_t is modeled by the differential equation

$$\rho V_t \frac{\mathrm{d}h_{dhw}}{\mathrm{d}t} = \dot{Q}_{he,dhw} - \dot{Q}_{dhw} - \dot{\hat{Q}}_{dhw}. \tag{B.8}$$

The mass flow $\dot{m}_{dhw}$ through the valve in front of the hot water heat exchanger is controlled by a *bang–bang* controller based on the temperature $T_{dhw} = {}^{h_{dhw}}/_{c_w}$ inside the storage tank

$$\dot{m}_{dhw} = \begin{cases} \dot{m}^{max}_{dhw}, & T_{dhw} \le T^{min}_{dhw} - 10\,^\circ\mathrm{C}, \\ 0.5\dot{m}^{max}_{dhw}, & T^{min}_{dhw} - 10\,^\circ\mathrm{C} < T_{dhw} \le T^{min}_{dhw} - 5\,^\circ\mathrm{C}, \\ 0.25\dot{m}^{max}_{dhw}, & T^{min}_{dhw} - 5\,^\circ\mathrm{C} < T_{dhw} \le T^{min}_{dhw}, \\ 0.125\dot{m}^{max}_{dhw}, & T^{min}_{dhw} < T_{dhw} \le 0.5\left(T^{max}_{dhw} - T^{min}_{dhw}\right), \\ 0\,\mathrm{kg\,s^{-1}}, & T^{max}_{dhw} < T_{dhw} \end{cases} \tag{B.9}$$

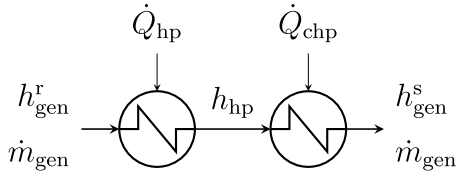

Fig. B.14. Serial HP and CHP connection.

with maximum and minimum temperature $T^{\max}_{\mathrm{dhw}} = 60\,°\mathrm{C}$ and $T^{\min}_{\mathrm{dhw}} = 40\,°\mathrm{C}$.

B.4. Generating unit

Within the simulation model implemented in *Modelica*, the generator is modeled by a heat exchanger and a pump. The heat exchanger dictates the supply temperature $T^{\mathrm{s}}_{\mathrm{gen}}$ of the DHN. The calculation of $T^{\mathrm{s}}_{\mathrm{gen}}$ is explained in Section 3.2.2.

The pressure control within a DHN is usually performed based on the supply pressure $p^{\mathrm{s}}_{\mathrm{cc}}$ and the return pressure $p^{\mathrm{r}}_{\mathrm{cc}}$ at the critical consumer [22]. In this work, a PI-controller is used to control the supply pressure $p^{\mathrm{s}}_{\mathrm{gen}}$ at the producer. The supply pressure is controlled to maintain the pressure difference $p^{\mathrm{s}}_{\mathrm{cc}} - p^{\mathrm{r}}_{\mathrm{cc}}$ at 2 bar. The pressure at the return junction of the producer is fixed at $p^{\mathrm{r}}_{\mathrm{gen}} = 6\,\mathrm{bar}$. Otherwise, the system of differential and algebraic equations would be underconstrained.

Based on the pressure control, the mass flow $\dot{m}_{\mathrm{gen}}(k)$ and the supply pressure $p^{\mathrm{s}}_{\mathrm{gen}}(k)$ at the generator are the result of each simulation at each time step k. Therefore, the electricity demand of the pump is given by

$$P_{\mathrm{pu}}(k) = \frac{1}{\rho \eta_{\mathrm{pu}}} \dot{m}_{\mathrm{gen}}(k) \left(p^{\mathrm{s}}_{\mathrm{gen}}(k) - p^{\mathrm{r}}_{\mathrm{gen}} \right) \tag{B.10}$$

with the pump efficiency $\eta_{\mathrm{pu}} = 0.8$ [26].

The CHP is modeled by

$$\dot{Q}_{\mathrm{gen}}(k) = \eta_{\mathrm{gth}} P_{\mathrm{gas}}(k), \tag{B.11a}$$

$$P_{\mathrm{chp}}(k) = \eta_{\mathrm{gtp}} P_{\mathrm{gas}}(k) \tag{B.11b}$$

with the two efficiencies $\eta_{\mathrm{gtp}} = 0.3$ and $\eta_{\mathrm{gth}} = 0.6$.

The required electric power

$$P_{\mathrm{hp}}(k) = \frac{1}{\mathrm{COP}(k)} \dot{Q}_{\mathrm{gen}}(k) \tag{B.12}$$

of the air source HP is calculated using a coefficient of performance (COP) [52]

$$\mathrm{COP}(k) = \eta_{\mathrm{c}} \frac{T_{\mathrm{hp}}(k) + \Delta T}{T_{\mathrm{hp}}(k) - T_{\mathrm{od}}(k) + 2\Delta T} \tag{B.13}$$

with $T_{\mathrm{hp}}(k) = 1/2 \left(T^{\mathrm{s}}_{\mathrm{gen}}(k) + T^{\mathrm{r}}_{\mathrm{gen}}(k) \right)$ and the temperature difference $\Delta T = 10\,\mathrm{K}$ taking into account the gradient between secondary fluids and refrigerant. The Carnot efficiency factor η_{c} is set to $\eta_{\mathrm{c}} = 0.488$ based on the data provided in [52].

Appendix C. Cost parameters

In this Section, the used DHN costs and parameters are condensed. Most data is taken from [51]. In order to compare the yearly operation cost of the DHN and the investment cost, the investment cost has to be annualized. This is achieved by

$$A_i = \sigma_{\mathrm{debt}} C_i \frac{r}{1 - (1 + +r)^{-w_i}} + \sigma_{\mathrm{equity}} \frac{C_i}{w_i} \tag{C.1}$$

with the investment cost C_i of matter of investment i, the debt ratio $\sigma_{\mathrm{debt}} = 0.29$, the equity ratio $\sigma_{\mathrm{equity}} = 0.71$ [53], and the interest rate $r = 0.04$ [26]. The lifetime w_i of i is depicted in Table C.3.

Table C.2
Pipe options taken from [54].

Type	U in $\mathrm{W\,m^{-1}\,K^{-1}}$	d in mm
DRE-20	0.1	16.5
DRE-25	0.118	20.9
DRE-32	0.128	29.6
DRE-40	0.144	35.5
DRE-50	0.159	47.5
DRE-65	0.179	63.3
DRE-80	0.188	76.1
DRE-100	0.194	99.9
DRE-125	0.223	125.3
DRE-150	0.253	152.3
DRE-175	0.268	175.7
DRE-200	0.276	201.1
DRE-225	0.292	224.5
DRE-250	0.308	253
DRE-300	0.324	301.5
DRE-350	0.341	333.2
DRE-400	0.357	381.2
DRE-450	0.373	431.8
DRE-500	0.390	482.8
DRE-550	0.406	533.6
DRE-600	0.422	581.6
DRE-650	0.439	631.6
DRE-700	0.455	679
DRE-750	0.471	730
DRE-800	0.488	777.8
DRE-850	0.504	828.8
DRE-900	0.520	874
DRE-1000	0.537	972

Table C.3
Assumed lifetimes used for annualizing investment costs taken from [3].

Type	Lifetime in a
HP	20
Pipe	40
House station	20
CHP	30
Pump	20

Table C.4
House station cost data taken from [51].

$\dot{Q}^{\mathrm{b}}_{\max}$ in kW	c_{hs} in €
≤20	6003
>20, ≤50	6353
>50, ≤100	6729
>100	7438

Table C.5
CHP and HP size options with cost data taken from [51].

g	$\dot{Q}^{g}_{\max}$ in MW	c_g in mil. € $\mathrm{MW^{-1}}$
CHP	0.545	0.89
	1.12	0.72
	2.02	0.73
	5.04	0.66
	9.393	0.65
	14.512	0.65
HP	0.3	1.522
	1.5	0.761
	5	0.609
	20	0.533

The total investment cost of the piping system C_{pi} is given by $C_{\mathrm{pi}} = \sum_{p \in \mathcal{G}_{\mathrm{dhn}}} c_{\mathrm{pi}} \ell(p)$, where $c_{\mathrm{pi}} = 1500\,€\,\mathrm{m^{-1}}$. The total house station cost $C_{\mathrm{hs}} = \sum_{b \in \mathcal{B}} c_{\mathrm{hs}} \left(\dot{Q}^{b}_{\max} \right)$ depend on the maximum heating power $\dot{Q}^{b}_{\max}$ of building b. The cost data c_{hs} is given in Table C.4.

The DHN pump cost $C_{\mathrm{pu}} = c_{\mathrm{pu}} \max_{k \in \mathcal{K}} P_{\mathrm{pu}}$ is assumed to increase linearly with the maximum pumping power, where $c_{\mathrm{pu}} = 72\,000\,€\,\mathrm{MW^{-1}}$ [51].

The investment cost of the producer is based on the maximum required heating power $\dot{Q}^{g}_{\max} = \max_{k\in\mathcal{K}} \dot{Q}_{g}(k)$ with the two generator types $g \in \{\text{hp}, \text{chp}\}$. From Table C.5 the smallest generation unit of type g with maximum heating power $\underline{\dot{Q}}^{g}_{\max}$ and specific cost c_g is selected such that $\underline{\dot{Q}}^{g}_{\max} \geq \dot{Q}^{g}_{\max}$. In case $\dot{Q}^{g}_{\max} = 0$, no generation unit of type g is required. Then, the generation unit cost is given by

$$C_{\text{gen}} = \sum_{g\in\{\text{hp,chp}\}} c_g\left(\underline{\dot{Q}}^{g}_{\max}\right)\underline{\dot{Q}}^{g}_{\max}. \tag{C.2}$$

Variables	
z	Planning variables
y	Expansion planning variables
u	Operation planning variables
$\mathcal{B}$	Set of building indices
Q	Heat demand in W h
$\dot{Q}$	Heating power in W
$\mathcal{G}$	Graph
$\mathcal{N}$	Set of nodes of a graph
$\mathcal{E}$	Set of edges of a graph
ℓ	Length of edge in m
β	Flexibility factor for constrained Steiner tree search
g	Graph node of generation unit
$\text{sp}(\mathcal{G}, g, n, \ell)$	Function for finding shortest path from g to n within $\mathcal{G}$ with the edge weight ℓ
$\text{msp}(\mathcal{G}, \mathcal{N}, g, \ell)$	Function for finding shortest path from any node in $\mathcal{N}$ to g within $\mathcal{G}$ with the edge weight ℓ. Returns the start node in $\mathcal{N}$ of the shortest path as well
p	Pressure in Pa
k	Time step
t	Time in h
T	Temperature in K or °C
λ	Pipe friction factor
ϵ	Pipe roughness in mm
d	Pipe diameter in m
Δ	Difference
η	Efficiency factor
$\dot{m}$	Mass flow in kg s^{-1}
P	Electric power
h	Enthalpy in J kg^{-1}
c_w	Heat capacity of water in $\text{J kg}^{-1}\text{ K}^{-1}$
ρ	Density of water in kg m^{-3}
U	Heat loss factor in $\text{W m}^{-1}\text{ K}^{-1}$
ν	Dynamic viscosity $\text{kg m}^{-1}\text{ s}^{-1}$
$\mathcal{K}$	Set of time steps
$\dot{\hat{Q}}$	Heat power losses in W
G	Thermal conductivity in W K^{-1}
R	Thermal resistance in K W^{-1}
C	Heat capacity in W h K^{-1}
A	Area in m^2
c	Specific cost in $€\,\text{W}^{-1}\text{ h}^{-1}$
V	Volume in m^3
J	Objective
γ	Heat losses in %
E	Energy in W h
n	Number of
ζ	Number of control volumes per length in km^{-1}
COP	Coefficient of performance of HP
σ	Annualization parameters
$\mathcal{Z}$	Set of input vectors of the parameter study

Subscripts	
s	Supply of the DHN
r	Return of the DHN
gen	Generation unit
max	Maximum
osm	Open street map
rou	Routing options
b	Buildings
cro	Street intersections
term	Terminal nodes
dhn	District heating network
st	Steiner minimal tree
$\sum$	Sum
cc	Critical consumer
sp	Shortest path
sim	Simulation model
pu	Pump
hs	House station
rh	Room heating
dhw	Domestic hot water
he	Heat exchanger
hc	Control curve
nom	Nominal value
t	Storage tank
hp	Heat pump
chp	Combined heat and power plant
od	Outdoor air
ele	Electricity
gas	Gas
CO_2	CO_2
opt	Operation
inv	Invest
pi	Pipe
comp	Computation
in	Input
out	Output
cv	Control volume
ju	Junction
so	Soil
gtp	Gas to power
gth	Gas to heat
c	Carnot
debt	Debt
equity	Equity

Abbreviations	
DHN	District heating network
OSM	Open street map
EH	Energy hub
TPL	Target pressure loss
DHW	Domestic hot water
CHP	Gas fueled combined heat and power unit
HP	Heat pump
COP	Coefficient of performance
CS	Constrained Steiner
CV	Control volume

Data availability

Data will be made available on request.

References

[1] European Commission. The European Green Deal. 2019.

[2] Fraunhofer Institute for Solar Energy Systems. Wege zu einem klimaneutralen Energiesystem. 2021.

[3] Lund H, Möller B, Mathiesen BV, Dyrelund A. The role of district heating in future renewable energy systems. Energy 2010;35(3):1381–90. http://dx.doi.org/10.1016/j.energy.2009.11.023.

[4] Heendeniya CB, Sumper A, Eicker U. The multi-energy system co-planning of nearly zero-energy districts – status-quo and future research potential. Appl Energy 2020;267:114953. http://dx.doi.org/10.1016/j.apenergy.2020.114953.

[5] Dochev I, Seller H, Peters I. Assigning Energetic Archetypes to a Digital Cadastre and Estimating Building Heat Demand. An Example from Hamburg, Germany. Environ Clim Technol 2020;24(1):233–53. http://dx.doi.org/10.2478/rtuect-2020-0014.

[6] Eslami S, Noorollahi Y, Marzband M, Anvari-Moghaddam A. District heating planning with focus on solar energy and heat pump using GIS and the supervised learning method: Case study of Gaziantep, Turkey. Energy Convers Manage 2022;269:116131. http://dx.doi.org/10.1016/j.enconman.2022.116131.

[7] Lund H, Thellufsen JZ. EnergyPLAN - Advanced Energy Systems Analysis Computer Model. 2020, http://dx.doi.org/10.5281/zenodo.4017214, Publisher: Zenodo.

[8] Klemm C, Vennemann P. Modeling and optimization of multi-energy systems in mixed-use districts: A review of existing methods and approaches. Renew Sustain Energy Rev 2021;135:110206. http://dx.doi.org/10.1016/j.rser.2020.110206.

[9] Prina MG, Groppi D, Nastasi B, Garcia DA. Bottom-up energy system models applied to sustainable islands. Renew Sustain Energy Rev 2021;152:111625. http://dx.doi.org/10.1016/j.rser.2021.111625.

[10] Guelpa E, Barbero G, Sciacovelli A, Verda V. Peak-shaving in district heating systems through optimal management of the thermal request of buildings. Energy 2017;137:706–14. http://dx.doi.org/10.1016/j.energy.2017.06.107.

[11] Guelpa E, Toro C, Sciacovelli A, Melli R, Sciubba E, Verda V. Optimal operation of large district heating networks through fast fluid-dynamic simulation. Energy 2016;102:586–95. http://dx.doi.org/10.1016/j.energy.2016.02.058.

[12] Fuchs M, Müller D. Automated Design and Model Generation for a District Heating Network from OpenStreetMap Data. In: Building simulation conference proceedings. IBPSA; 2017, p. 2050–9. http://dx.doi.org/10.26868/25222708.2017.562.

[13] Gilbert EN, Pollak HO. Steiner Minimal Trees. SIAM J Appl Math 1968;16(1):1–29. http://dx.doi.org/10.1137/0116001, Publisher: Society for Industrial and Applied Mathematics.

[14] Kou L, Markowsky G, Berman L. A fast algorithm for Steiner trees. Acta Inform 1981;15(2):141–5. http://dx.doi.org/10.1007/BF00288961, Publisher: Springer; Springer-Verlag.

[15] Mehlhorn K. A faster approximation algorithm for the Steiner problem in graphs. Inform Process Lett 1988;27(3):125–8. http://dx.doi.org/10.1016/0020-0190(88)90066-X.

[16] Vieth J, Westphal J, Speerforck A. A GIS-based co-planning approach for district heating networks. Energy Proc 2024;50. http://dx.doi.org/10.46855/energy-proceedings-11423.

[17] Lund H, Werner S, Wiltshire R, Svendsen S, Thorsen JE, Hvelplund F, Mathiesen BV. 4th Generation District Heating (4GDH): Integrating smart thermal grids into future sustainable energy systems. Energy 2014;68:1–11. http://dx.doi.org/10.1016/j.energy.2014.02.089.

[18] Résimont T, Louveaux Q, Dewallef P. Optimization Tool for the Strategic Outline and Sizing of District Heating Networks Using a Geographic Information System. Energies 2021;14(17):5575. http://dx.doi.org/10.3390/en14175575, Publisher: Multidisciplinary Digital Publishing Institute.

[19] Sartor K, Quoilin S, Dewallef P. Simulation and optimization of a CHP biomass plant and district heating network. Appl Energy 2014;130:474–83. http://dx.doi.org/10.1016/j.apenergy.2014.01.097.

[20] Blommaert M, Wack Y, Baelmans M. An adjoint optimization approach for the topological design of large-scale district heating networks based on nonlinear models. Appl Energy 2020;280:116025. http://dx.doi.org/10.1016/j.apenergy.2020.116025.

[21] Wack Y, Baelmans M, Salenbien R, Blommaert M. Economic topology optimization of District Heating Networks using a pipe penalization approach. Energy 2023;264:126161. http://dx.doi.org/10.1016/j.energy.2022.126161, Num Pages: 10.

[22] Frederiksen S, Werner S. District heating and cooling. Studentlitteratur; 2013.

[23] Narula SC, Ho CA. Degree-constrained minimum spanning tree. Comput Oper Res 1980;7(4):239–49. http://dx.doi.org/10.1016/0305-0548(80)90022-2.

[24] Talebi B, Mirzaei PA, Bastani A, Haghighat F. A Review of District Heating Systems: Modeling and Optimization. Front Built Environ 2016;2:22. http://dx.doi.org/10.3389/fbuil.2016.00022.

[25] Morvaj B, Evins R, Carmeliet J. Optimising urban energy systems: Simultaneous system sizing, operation and district heating network layout. Energy 2016;116:619–36. http://dx.doi.org/10.1016/j.energy.2016.09.139.

[26] Hering D, Xhonneux A, Müller D. Design optimization of a heating network with multiple heat pumps using mixed integer quadratically constrained programming. Energy 2021;226:120384. http://dx.doi.org/10.1016/j.energy.2021.120384.

[27] Hauk C, Ulbig A, Moser A. Integrated planning of grids and energy conversion units in municipal multi-energy carrier systems. Energy Inform 2021;4(S3). http://dx.doi.org/10.1186/s42162-021-00178-0.

[28] Wirtz M, Heleno M, Moreira A, Schreiber T, Müller D. 5Th generation district heating and cooling network planning: A Dantzig–Wolfe decomposition approach. Energy Convers Manage 2023;276:116593. http://dx.doi.org/10.1016/j.enconman.2022.116593.

[29] Wirtz M. nPro: A web-based planning tool for designing district energy systems and thermal networks. Energy 2023;268:126575. http://dx.doi.org/10.1016/j.energy.2022.126575.

[30] Geidl M, Koeppel G, Favre-Perrod P, Klockl B, Andersson G, Frohlich K. Energy hubs for the future. IEEE Power Energy Mag 2007;5(1):24–30. http://dx.doi.org/10.1109/MPAE.2007.264850.

[31] Falke T, Krengel S, Meinerzhagen A-K, Schnettler A. Multi-objective optimization and simulation model for the design of distributed energy systems. Appl Energy 2016;184:1508–16. http://dx.doi.org/10.1016/j.apenergy.2016.03.044.

[32] Blesl M, Stehle M, Broydo M. EnEff: Wärme - Planungsinstrumente für zukünftige Niedertemperatur-Fernwärmeversorgungssysteme : im Rahmen des IEA implementing agreement DHC annex TS I. Technical report, Stuttgart: IER Institut für Energiewirtschaft und Rationelle Energieanwendung; 2017, http://dx.doi.org/10.2314/GBV:1018668012.

[33] Kuntuarova S, Lickleder T, Huynh T, Zinsmeister D, Hamacher T, Perić V. Design and simulation of district heating networks: A review of modeling approaches and tools. Energy 2024;305:132189. http://dx.doi.org/10.1016/j.energy.2024.132189.

[34] Lohmeier D, Cronbach D, Drauz SR, Braun M, Kneiske TM. Pandapipes: An open-source piping grid calculation package for multi-energy grid simulations. Sustainability 2020;12(23):9899. http://dx.doi.org/10.3390/su12239899.

[35] Transsolar Energietechnik GmbH. TRNSYS. 2025, URL: https://trnsys.de/en. [Accessed 12 May 2025].

[36] Fischer-Uhrig Engineering GmbH. STANET: network analysis. 2025, URL: http://stafu.de/en/home.html. [Accessed 12 May 2025].

[37] Dassault Systèmes. Dymola. 2025, URL: https://www.3ds.com/products/catia/dymola. [Accessed 12 May 2025].

[38] Pirouti M, Bagdanavicius A, Ekanayake J, Wu J, Jenkins N. Energy consumption and economic analyses of a district heating network. Energy 2013;57:149–59. http://dx.doi.org/10.1016/j.energy.2013.01.065.

[39] OpenStreetMap contributors. Planet dump. 2017, retrieved from https://planet.osm.org https://www.openstreetmap.org.

[40] Boeing G. Modeling and analyzing urban networks and amenities with OSMnx. Working paper, 2024, URL: https://geoffboeing.com/publications/osmnx-paper/.

[41] Kays J, Seack A, Smirek T, Westkamp F, Rehtanz C. The Generation of Distribution Grid Models on the Basis of Public Available Data. IEEE Trans Power Syst 2017;32(3):2346–53. http://dx.doi.org/10.1109/TPWRS.2016.2609850, Conference Name: IEEE Transactions on Power Systems.

[42] Hagberg AA, Schult DA, Swart PJ. Exploring Network Structure, Dynamics, and Function using NetworkX. In: Varoquaux G, Vaught T, Millman J, editors. Proceedings of the 7th python in science conference. Pasadena, CA USA; 2008, p. 11–5.

[43] Westphal J, Brunnemann J, Speerforck A. Enabling the dynamic simulation of an unaggregated, meshed district heating network with several thousand substations. Energy 2025;135434. http://dx.doi.org/10.1016/j.energy.2025.135434.

[44] 50Hertz Transmission GmbH, Amprion GmbH, TenneT TSO GmbH, TransnetBW GmbH. Netzentwicklungsplan Strom 2037 mit Ausblick 2045: Erster Entwurf der Übertragungsnetzbetreiber. 2023.

[45] Borges CLT, Martins VF. Multistage expansion planning for active distribution networks under demand and Distributed Generation uncertainties. Int J Electr Power Energy Syst 2012;36(1):107–16. http://dx.doi.org/10.1016/j.ijepes.2011.10.031.

[46] Lu H, Alanne K, Martinac I. Energy quality management for building clusters and districts (BCDs) through multi-objective optimization. Energy Convers Manage 2014;79:525–33. http://dx.doi.org/10.1016/j.enconman.2013.12.051.

[47] Queipo NV, Haftka RT, Shyy W, Goel T, Vaidyanathan R, Kevin Tucker P. Surrogate-based analysis and optimization. Prog Aerosp Sci 2005;41(1):1–28. http://dx.doi.org/10.1016/j.paerosci.2005.02.001.

[48] Strehle F, Vieth J, Pfeifer M, Hohmann S. Passivity-Based Stability Analysis of Hydraulic Equilibria in 4th Generation District Heating Networks. IFAC- Pap 2021;54(19):261–6. http://dx.doi.org/10.1016/j.ifacol.2021.11.088.

[49] Cerbe G, Lendt B. Grundlagen der Gastechnik. Hanser eLibrary, 8th ed.. München: Carl Hanser Verlag GmbH & Co. KG; 2016, http://dx.doi.org/10.3139/9783446449664.

[50] Gustafsson J, Delsing J, van Deventer J. Improved district heating substation efficiency with a new control strategy. Appl Energy 2010;87(6):1996–2004. http://dx.doi.org/10.1016/j.apenergy.2009.12.015.

[51] Ministry of the Environment, Climate Protection and the Energy Sector Baden-Württemberg. Kommunale Wärmeplanung: Einführung in den Technikkatalog. 2023.

[52] Jesper M, Schlosser F, Pag F, Walmsley TG, Schmitt B, Vajen K. Large-scale heat pumps: Uptake and performance modelling of market-available devices. Renew Sustain Energy Rev 2021;137:110646. http://dx.doi.org/10.1016/j.rser.2020.110646.

[53] Oliva H. S, Garcia G. M. Investigating the impact of variable energy prices and renewable generation on the annualized cost of hydrogen. Int J Hydrog Energy 2023;48(37):13756–66. http://dx.doi.org/10.1016/j.ijhydene.2022.12.304.

[54] REHAU GmbH. Technische Information – vorisolierte REHAU Systeme für die Wärme- & Kälteversorgung. Technical report, REHAU GmbH; 2020.